



HAL
open science

Modeling Transport of Cesium in Grimsel Granodiorite With Micrometer Scale Heterogeneities and Dynamic Update of K_d

Mikko Voutilainen, Pekka Kekäläinen, Marja Siitari-Kauppi, Paul Sardini,
Eveliina Muuri, Jussi Timonen, Andrew V Martin

► **To cite this version:**

Mikko Voutilainen, Pekka Kekäläinen, Marja Siitari-Kauppi, Paul Sardini, Eveliina Muuri, et al.. Modeling Transport of Cesium in Grimsel Granodiorite With Micrometer Scale Heterogeneities and Dynamic Update of K_d . Water Resources Research, 2017, 53 (11), pp.9245 - 9265. 10.1002/2017WR020695 . hal-01934967

HAL Id: hal-01934967

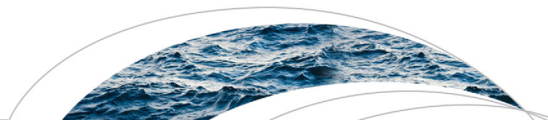
<https://hal.science/hal-01934967>

Submitted on 23 Sep 2021

HAL is a multi-disciplinary open access archive for the deposit and dissemination of scientific research documents, whether they are published or not. The documents may come from teaching and research institutions in France or abroad, or from public or private research centers.

L'archive ouverte pluridisciplinaire **HAL**, est destinée au dépôt et à la diffusion de documents scientifiques de niveau recherche, publiés ou non, émanant des établissements d'enseignement et de recherche français ou étrangers, des laboratoires publics ou privés.

Copyright



RESEARCH ARTICLE

10.1002/2017WR020695

Modeling Transport of Cesium in Grimsel Granodiorite With Micrometer Scale Heterogeneities and Dynamic Update of K_d

Mikko Voutilainen¹, Pekka Kekäläinen¹, Marja Siitari-Kauppi¹, Paul Sardini², Eveliina Muuri¹, Jussi Timonen³, and Andrew Martin⁴

¹Department of Chemistry, University of Helsinki, Helsinki, Finland, ²Institute of Chemistry, University of Poitiers, Poitiers, France, ³Department of Physics, University of Jyväskylä, Jyväskylä, Finland, ⁴National Cooperative for the Disposal of Radioactive Waste, Wetingen, Switzerland

Key Points:

- Heterogeneous mineral structure has a significant effect to transport of cesium in Grimsel granodiorite
- Time Domain Random Walk modeling in heterogeneous rock was able to reproduce similar diffusion profiles as in situ experiments
- Experimental structure characterization methods are essential when creating geometries for transport modeling

Correspondence to:

M. Voutilainen, ma.voutilainen@helsinki.fi

Citation:

Voutilainen, M., Kekäläinen, P., Siitari-Kauppi, M., Sardini, P., Muuri, E., Timonen, J., & Martin, A. (2017). Modeling transport of cesium in Grimsel granodiorite with micrometer scale heterogeneities and dynamic update of K_d . *Water Resources Research*, 53, 9245–9265. <https://doi.org/10.1002/2017WR020695>

Received 2 MAR 2017

Accepted 7 SEP 2017

Accepted article online 9 OCT 2017

Published online 16 NOV 2017

Abstract Transport and retardation of cesium in Grimsel granodiorite taking into account heterogeneity of mineral and pore structure was studied using rock samples overcored from an in situ diffusion test at the Grimsel Test Site. The field test was part of the Long-Term Diffusion (LTD) project designed to characterize retardation properties (diffusion and distribution coefficients) under in situ conditions. Results of the LTD experiment for cesium showed that in-diffusion profiles and spatial concentration distributions were strongly influenced by the heterogeneous pore structure and mineral distribution. In order to study the effect of heterogeneity on the in-diffusion profile and spatial concentration distribution, a Time Domain Random Walk (TDRW) method was applied along with a feature for modeling chemical sorption in geological materials. A heterogeneous mineral structure of Grimsel granodiorite was constructed using X-ray microcomputed tomography (X- μ CT) and the map was linked to previous results for mineral specific porosities and distribution coefficients (K_d) that were determined using C-14-PMMA autoradiography and batch sorption experiments, respectively. After this the heterogeneous structure contains information on local porosity and K_d in 3-D. It was found that the heterogeneity of the mineral structure on the micrometer scale affects significantly the diffusion and sorption of cesium in Grimsel granodiorite at the centimeter scale. Furthermore, the modeled in-diffusion profiles and spatial concentration distributions show similar shape and pattern to those from the LTD experiment. It was concluded that the use of detailed structure characterization and quantitative data on heterogeneity can significantly improve the interpretation and evaluation of transport experiments.

1. Introduction

A large amount of spent nuclear fuel (according to IAEA, 2008 by the end of 2005 about 180,000 MTHM) is being produced by nuclear power plants all around the world and the fuel consists of highly radioactive fission and activation products as well as uranium oxide and accumulated nuclides from decay series of uranium. The spent fuel contains many cesium isotopes: ¹³⁴Cs ($t_{1/2} = 2.07$ a), ¹³⁷Cs ($t_{1/2} = 30.7$ a), long living isotope ¹³⁵Cs ($t_{1/2} = t_{1/2} = 2.3 \cdot 10^6$ a), and stable isotope ¹³³Cs. Stable isotope ¹³³Cs is not dangerous for nature and it is a relatively rare element in the crust (Turekian & Wedepohl, 1959). However, the isotope ¹³⁵Cs is one of the critical radionuclides when considering the long-term safety of spent nuclear fuel repositories due to its long half-life (Posiva, 2013). Second, ¹³⁷Cs is one of the most important radionuclides for operational safety of nuclear power plants due to its high radiotoxicity (Amano et al., 1999; Hirose, 2012; Ohta et al., 2012; Sanada et al., 2002). To this end, it is important to study the behavior of cesium in contact with groundwater and bedrock. The isotopes ¹³⁴Cs and ¹³⁷Cs are typically used in the experiments that aim to study the transport of cesium due to their relatively short half-life and the fact that the data can also be used when interpreting the behavior of ¹³⁵Cs since their chemical and physical properties are identical.

In many countries (e.g., Finland, Sweden, Korea, and Czech Republic), crystalline rock has been chosen to be the host medium for underground repositories of spent nuclear fuel. For performance assessment and safety analysis of such repositories, it is vital to determine properties linked to the migration of radionuclides in the surrounding geosphere. In order to determine the diffusion and distribution coefficient (i.e., retardation properties) of bedrock in conditions which are analogous to those at repository sites, an in situ field test of the Long-Term Diffusion (LTD) experiment was setup in the Grimsel Test Site (GTS) in

Switzerland. A few similar in situ experiments with an aim to determine these properties in crystalline rock have been performed in Switzerland, Canada, Sweden, and Finland (Cvetkovic et al., 2007; Hadermann & Heer, 1996; Vilks et al., 2003; Voutilainen et al., 2014; Widestrand et al., 2010). In the LTD experiment, a cocktail of radionuclides (^3H as HTO, ^{22}Na , ^{134}Cs , and ^{131}I) was circulated in a 0.7 m long packed-off test-interval of a borehole (Soler et al., 2015). During the experiment, the concentration decrease of radionuclides was measured. After the experiment, the test-interval section was removed by overcoring with a wide diameter drill-bit and the in-diffusion profiles of radionuclides in the rock core were determined in the laboratory using a variety of techniques (Ikonen et al., 2016a; Jokelainen et al., 2013; Soler et al., 2015). From these measurements, porosity of the rock and effective diffusion coefficients and distribution coefficients of the radionuclides in the Grimsel granodiorite were determined and the results were compared to ones from laboratory experiments (Ikonen et al., 2017; Tachi et al., 2015). The spatial concentration distribution of ^{134}Cs was studied qualitatively using autoradiography (Jokelainen et al., 2013). It was observed that ^{134}Cs had diffused up to a depth of 1.5 cm and that heterogeneous spatial concentration distribution was strongly influenced by the heterogeneous mineral structure due to a significant sorption of ^{134}Cs on mica rich areas. Similar spatial concentration distributions of cesium and influence of significant sorption on mica rich areas have been observed also in other in situ experiments (Nilsson et al., 2010; Widestrand et al., 2007). The results of the aforementioned studies have only been analyzed previously using simple homogeneous or dual-component models even though autoradiography has shown more complex spatial concentration distributions that cannot be reproduced with such simple models.

A number of laboratory experiments have been performed in which diffusion and distribution coefficients of cesium in crystalline rock samples have been determined (Ittner et al., 1990; Kyllönen et al., 2014; Puukko, 2014; Skagius & Neretnieks, 1988; Tachi et al., 2011; Tachi and Yotsuji, 2014; Videnská et al., 2015). In addition to the in situ experiments mentioned above, transport experiments performed in the laboratory have also shown strongly heterogeneous spatial concentration distribution of cesium (Johansson et al., 1998; Puukko, 2014). From these studies, it has been concluded that the sorption of cesium is strongly mineral dependent and that the heterogeneity of the distribution is a consequence of the heterogeneity of the mineral structure. Multiple studies have been performed to quantify the mineral dependency of sorption by measuring mineral specific distribution coefficients of cesium on common minerals found in crystalline rocks (Byegård et al., 1995; Muuri et al., 2016, 2017; Pinnioja et al., 1983; Sasaki et al., 2007; Tsukamoto & Ohe, 1993). In general, the heterogeneity of mineral and pore structure of the rock on the centimeter scale may have a considerable influence on the transport properties and these heterogeneities may also be present on multiple scales in crystalline rock.

Previously, diffusion in heterogeneous rock has been modeled using, e.g., Continuous Time Random Walk (CTRW) models (Gouze et al., 2008; Noetinger & Estebenet, 2000), lattice-Boltzmann simulations (Genty & Pot, 2014; Jeong et al., 2008; Xuan et al., 2010), or commercial tools for solving partial differential equations of transport problems (Glaus et al., 2015; Ganapathysubramanian & Zabarar, 2007). In addition to these methods, many others have been applied when advection, dispersion, and chemical reactions are affecting the transport (Berkowitz et al., 2000; Blessent et al., 2011; Cvetkovic et al., 1999, 2010; Dentz et al., 2011; Kuva et al., 2016; Mettier et al., 2006; Kekäläinen et al., 2011; Toivanen et al., 2013; Trincherro et al., 2015; Voutilainen et al., 2010). As the changes in chemical conditions may affect local diffusion and distribution coefficients, new methods allowing values to be dynamically updated (Trincherro et al., 2016) and a so-called smart- K_d concept (Flügge et al., 2013; Noseck et al., 2014) have been developed for solving the problem on a large scales. In the aforementioned studies, geochemical models are coupled with transport models to study the transport of radionuclides under transient conditions.

One possibility to handle heterogeneities on the centimeter scale is to apply a Time Domain Random Walk (TDRW) method which has been developed for simulating transport of elements in heterogeneous media (Delay et al., 2002; Delay & Porel, 2003; McCarthy, 1993). The method is a time domain realization of particle random walks that enables simulation of diffusion in heterogeneous media when the local porosities and diffusion coefficients are known. The TDRW method has been used to study the effect of centimeter scale structural heterogeneities on diffusion in various cases (Robinet et al., 2008, 2012; Sardini et al., 2007; Voutilainen et al., 2013). The TDRW method has also been found to be a powerful tool for analyzing results from both in situ and laboratory experiments especially when the initial or boundary conditions are complicated (Ikonen et al., 2016b, 2017; Soler et al., 2014). Previously Dentz et al. (2012) have modified the TDRW

method by including sorption of diffusing elements in heterogeneous media. Sorption is not defined to support distribution coefficients that are typically measured for geological media. Furthermore, the TDRW method has been developed further by including advection in fractured media (Gjetvaj et al., 2015; Klepikova et al., 2016; Noetinger et al., 2016; Russian et al., 2016). However, in previous studies, TDRW method has not been used with a dynamic update of local parameters or in the smart- K_d concept.

In order to generate a realistic medium for the transport simulations, structure characterization methods such as X-ray microcomputed tomography (X- μ CT; Sasov & Van Dyck, 1998; Schladitz, 2011) and C-14-labeled-polymethylmethacrylate (C-14-PMMA) autoradiography (Hellmuth et al., 1993, 1994; Sardini et al., 2006) are essential. Rapid development in the spatial resolution and technology of X- μ CT scanners and in the reconstruction algorithms has greatly increased the possible use of the method in research applications of geomaterials (Cnudde & Boone, 2013; Fuisse et al., 2014). In addition, recent developments of C-14-PMMA autoradiography, which can resolve spatial porosity distribution in micrometer scale on centimeter scale samples, have broadened the field of applications and increased the feasibility of the technique (Sammaljärvi et al., 2012, 2016; Sardini et al., 2015). Previously Voutilainen et al. (2012) have introduced a novel combination of these methods with scanning electron microscopy to characterize the 3-D mineral and porosity map of crystalline rock sample. However, studies that combine these structure characterization methods with batch sorption experiments do not exist.

In this study, the approach developed by Dentz et al. (2012) has been applied and developed further so that the distribution and diffusion coefficient, which are typically measured in geological media, can be utilized in transport simulations of cesium performed with the TDRW method. In addition, we have included an option for taking into account the concentration-dependent distribution coefficient in the TDRW method which has not been proposed before. Validation of these novel properties of the TDRW method has also been performed to build confidence in the results. In order to create a realistic 3-D mineral and pore structure for the TDRW simulations, the X- μ CT and C-14-PMMA autoradiography were applied and the results were combined using the methods by Voutilainen et al. (2012). Furthermore, the methods were developed further so that mineral specific distribution coefficients determined by Muuri et al. (2016) can be utilized in reactive transport modeling presented here. We have applied these features to model diffusion of cesium in a realistic mineral and pore structure of Grimsel granodiorite taking into account the mineral specific and concentration-dependent sorption properties. The aims of these modeling tasks has been to (i) investigate the impacts of microscale mineral and structure heterogeneity on cesium transport in Grimsel granodiorite, (ii) test if results from such a model lead to similar heterogeneous spatial concentration distributions and in-diffusion profiles as has been observed in the previous laboratory and in situ experiments, and (iii) demonstrate how dynamically changing local distribution coefficients affect in-diffusion profiles.

2. Materials and Methods

2.1. Rock Samples

The main rock types at the GTS are Aare granite and Grimsel granodiorite, the latter being studied here. The Grimsel granodiorite is medium grained and mainly composed of K-feldspar (12–24%), plagioclase (29–30%), quartz (27–28%), and biotite (7–11%) with accessory muscovite/sericite, apatite, sphene, epidote, zircon, chlorite, calcite, and opaques (Möri et al., 2003). Furthermore, Schild et al. (2001) and Möri et al. (2003) have done extensive petrographic, structural, and porosity analyzes from rock samples that have been taken from less than 5 m from the samples analyzed here. It can be assumed that these properties do not change considerably within this distance. The samples studied here were taken from a drill hole in vicinity of a previous in situ resin injection study site. A shear zone that intersects the tunnel with an orientation of 144/80 (dip direction/dip angle) intersects also the drill hole at 3.02 m (Kelokaski et al., 2006; Möri et al., 2003). According to Möri et al. (2003), the shear zone does not affect considerably the petrography of rock within the studied distance and, more importantly, Kelokaski et al. (2006) found out that it does not affect considerably the porosity or pore structure of rock.

A $19 \times 18 \times 15$ mm³ rock sample was sawn from the drill core for structural characterization using X- μ CT with a diamond saw. The sample was sawn from the middle of the drill core and the location was selected so that weak orientation of biotite grains could be observed from the sawn surfaces. Such orientation of biotite was also observed in a previous study (Möri et al., 2003) and may form pathways that cause some

Table 1
The Total Porosity of Grimsel Granodiorite and Intramineral Porosities of Major Minerals Determined by a Combination of C-14-PMMA Autoradiography and the Separation of Mineral Phases (Kelokaski et al., 2006) and Distribution Coefficients Determined in a Cesium Concentration of 10^{-8} M (Muuri et al., 2016)

	Porosity (%)	Distribution coefficient (m^3/kg)
Grimsel granodiorite	0.69	0.107 ± 0.003
Plagioclase	0.66	0.18 ± 0.04
Quartz	0.68	
K-feldspar	0.70	0.0368 ± 0.0004
Biotite	0.88	0.304 ± 0.005

preferential directions for transport. It is possible to study also the effect of biotite orientation with the selected sample.

In addition, Kelokaski et al. (2006) determined intramineral porosities for the major minerals of Grimsel granodiorite (see Table 1). In their work, they first determined the spatial distribution of porosity of the rock surface using C-14-PMMA autoradiography (Hellmuth et al., 1993, 1994; Siitari-Kauppi, 2002). They applied the method by Sardini et al. (2006) for the digital separation of mineral phases, superimposing the spatial distribution of porosity with a mineral map and determined intramineral porosities. They found that the porosity of Grimsel granodiorite is mainly intramineral pore spaces with a small amount of intermineral pores at grain boundaries as well as a few microfissures transecting the mineral grains. Previously, Muuri et al. (2016) have determined mineral specific distribution coefficients of cesium for the major minerals of Grimsel granodiorite using traditional batch sorption experiments (see Table 1). They performed the measurements on crushed minerals as a function of cesium concentration using a synthetic Grimsel groundwater simulant (Mäder et al., 2006) in order to mimic the chemical groundwater conditions at the GTS. They have also used a PHREEQC model to explain the measured curve for the distribution coefficient of cesium on biotite as a function of concentration. Furthermore, they found that the distribution coefficient of cesium on quartz was negligibly small and that the decreasing trends for distribution coefficients of cesium on plagioclase and K-feldspar were similar. They also performed the same measurement using crushed Grimsel granodiorite containing all of the mineral constituents.

The effective diffusion coefficients (D_e) of radionuclides in Grimsel granodiorite have been determined in several studies from the LTD experiment and from similar laboratory experiments (see Table 2). Based on these studies D_e of $3 \times 10^{-12} m^2/s$ was chosen for HTO and ^{134}Cs for modeling since the focus was mainly on the effect of chemical heterogeneity on the spatial concentration distribution of cesium and its in-diffusion profile.

2.2. X-Ray Computed Tomography at Micrometer Scale

The 3-D mineral structure of the sample was determined using X- μ CT. Sample preparation, X- μ CT scanning, image reconstruction, noise filtering, and image segmentation were all taken into account (Voutilainen et al., 2012). In this study, X- μ CT scanning was done with a XRadia Micro XCT 400 scanner which has a

Table 2
Effective Diffusion Coefficients (D_e) of Different Nuclides in Intact Grimsel Granodiorite Reported in Previous Studies

Nuclide	D_e (m^2/s)	Experiment	Reference
^{134}Cs	3×10^{-12}	LTD in situ	Jokelainen et al. (2013)
^{134}Cs	$3-4 \times 10^{-12}$	LTD in situ	Soler et al. (2015)
^{134}Cs	2.37×10^{-12}	LTD in situ	Tachi et al. (2015)
^{134}Cs	8.08×10^{-12}	Laboratory	Tachi et al. (2015)
HTO	$1.7-2.0 \times 10^{-13}$	LTD in situ	Soler et al. (2015)
HTO	$2 \times 10^{-12} m^2/s$	LTD in situ	Ikonen et al. (2016b)
HTO	7.21×10^{-13}	LTD in situ	Tachi et al. (2015)
HTO	2.64×10^{-12}	Laboratory	Tachi et al. (2015)
He ^a	2.3×10^{-12}	Laboratory	Kuva et al. (2015)

^aValue has been converted from gas phase to the water phase by using a factor of 11,600 (Hartikainen et al., 1996).

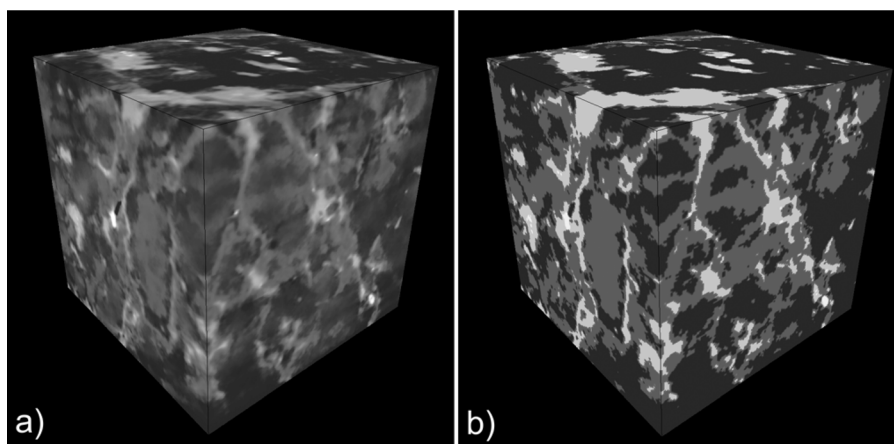


Figure 1. 3-D visualization of (a) original and (b) segmented tomograms of the Grimsel granodiorite sample. Visualizations include quartz (dark gray), feldspars (gray), and biotite (light gray). The dimensions of the sample are $14 \times 14 \times 14 \text{ mm}^3$.

conventional X-ray tube with a spot size less than $7 \mu\text{m}$ and a conical X-ray beam. The sample was scanned using a pixel resolution of $20.0 \mu\text{m}$, acceleration voltage of 90 kV, and magnification of 0.5. During the scan, 2,000 projections were taken with total rotation of 186° . The reconstructed 3-D image was done using commercial software (Xradia TXM Reconstructor). After the reconstruction, a 3-D realization of a nonlinear variance-based noise-reduction filter was applied to the 3-D image (Gonzalez & Woods, 2002). For segmentation of different minerals, a k -mean cluster algorithm in gray value space ($k = 3$) was applied (Forsyth & Ponce, 2002). Seed pixels were selected manually from the surface, distances were determined as Euclidean distances, and the algorithm was terminated when no pixels were changed in the cluster.

2.2.1. Construction of Simulation Geometry

The simulation geometry with constant cell size was constructed following the procedure reported by Voutilainen et al. (2012). Tomographic imaging was done for the whole of the Grimsel granodiorite sample and from a subsample of $14 \times 14 \times 14 \text{ mm}^3$ was cropped for further use. The voxel size of the geometry was decreased to $80 \mu\text{m}$ in order to reduce memory usage and calculation time of the TDRW modeling. In Figure 1, the resulting visualization of the original and segmented 3-D tomograms is shown. The segmented tomogram can be considered as a 3-D mineral map of the Grimsel granodiorite sample containing quartz (dark gray), feldspars (gray), and biotite (light gray). Unfortunately, the gray values of plagioclase and K-feldspar overlapped due to similar X-ray attenuation coefficients and thus they could not be distinguished from each other and are merged into one mineral phase in the 3-D mineral map. Fortunately, their transport properties are rather similar compared to that of biotite and quartz, and thus they are treated as one mineral group of feldspar. When the mineral map is linked to the mineral specific porosity data (see Table 1), the 3-D tomogram of Grimsel granodiorite can be used also as a 3-D porosity map. As the plagioclase and K-feldspar are merged into feldspar in the mineral map, the porosity of feldspar was determined to be 0.68%. This was performed using average porosities from Table 1 and total abundances.

In a previous study, Muuri et al. (2016) determined the distribution coefficients of cesium in the major minerals of Grimsel granodiorite as a function of cesium concentration. They have presented an exact fit for biotite by PHREEQC modeling. In order to apply the rest of their results in our work, we have fitted a function $K_d = a_1 + a_2 C^{a_3}$ to their measurement data for plagioclase, K-feldspar, and Grimsel granodiorite (see Figure 2). Here a_1 , a_2 , and a_3 were used as fitting parameters. In Figure 2a, combined fit for plagioclase and K-feldspar is also shown since their gray values overlapped in the 3-D tomogram. The combined data and fit were determined by multiplying individual data of minerals by the ratio of abundance of mineral and their sum abundance. After this, the mineral and concentration-dependent distribution coefficients could be linked to the 3-D mineral map.

2.3. Time Domain Random Walk

The 3-D image created using the methods described above was applied in TDRW simulations. The method is formulated in a Lagrangian context with finite volume and it is described here only briefly. A more

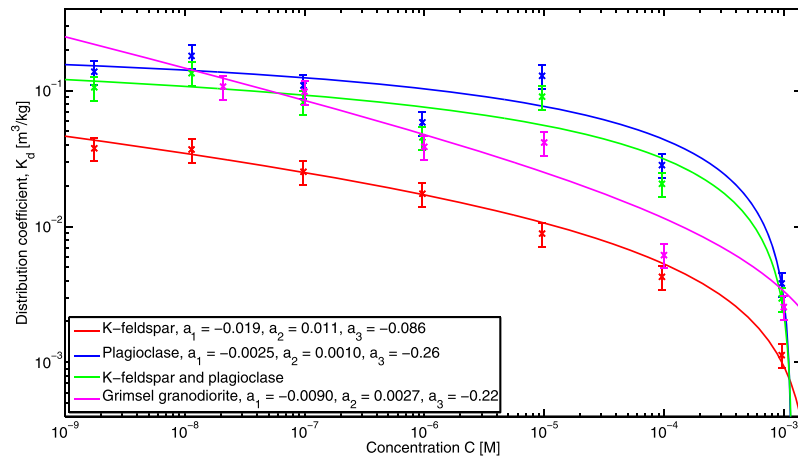


Figure 2. The distribution coefficients of cesium as a function of concentration on Grimsel granodiorite (magenta), plagioclase (blue), and K-feldspar (red) fitted by $K_d = a_1 + a_2 C^{a_3}$. The combined fit (green) of plagioclase and K-feldspar takes into account the real averaged mineral abundances.

detailed description is given by Delay et al. (2002), Delay and Porel (2003), Sardini et al. (2003), and Voutilainen et al. (2013). In general, the method is convenient when dealing with large systems since the computation times do not considerably depend on sample size, and it is faster than more traditional simulation methods (Sardini et al., 2003). Here the particle, which represents a diffusing molecule, is forced to jump during a transition time to one of its neighboring voxels. In the TDRW method, a particle in voxel i jumps to neighboring voxel j with a transition probability determined from:

$$P_{ij} = \frac{b_{ij}}{\sum_j b_{ij}}, \tag{1}$$

where

$$b_{ij} = \frac{A_{ij}(\epsilon D_p)_{ij}}{L_{ij}} = \frac{A_{ij}(D_e)_{ij}}{L_{ij}} \tag{2}$$

with A_{ij} the total area between voxels i and j , $(\epsilon D_p)_{ij}$ the harmonic mean of the product of porosity (ϵ) and local pore diffusion coefficient (D_p) at voxels i and j , and L_{ij} the distance between the centers of voxels i and j . After the transition direction has been defined according to transition probabilities, a transition time for a jump from voxel i to voxel j is given by

$$t_{i \rightarrow j} = - \frac{\epsilon_i V_i}{\sum_j b_{ij}} \log(u_{01}), \tag{3}$$

where V_i is the total volume of voxel i and u_{01} a random number from a uniform distribution between 0 and 1. The equations described above do not take chemical sorption into account and thus are not directly applicable when studying the transport of cesium in crystalline rock. Dentz et al. (2012) modified the TDRW method so that the sorption and desorption of particles can be taken into account. They proposed that the transition time between two positions for sorbing element ($T_{i \rightarrow j}$) is simply a sum of times during which the particle is mobile ($t_{i \rightarrow j}$) and sorbed (t_s). They also introduced a trapping frequency and distributions for trapping time and number of trappings during $t_{i \rightarrow j}$ which could be used to mimic chemical sorption and desorption. However, trapping frequency and these distributions are difficult to measure for natural materials. Thus we propose a form for sorption time during the transition:

$$t_s = - \frac{\epsilon_i V_i}{\sum_j w_{ij}} \log(u_{01}) - \left(- \frac{\epsilon_i V_i}{\sum_j b_{ij}} \log(u_{01}) \right), \tag{4}$$

where

$$w_{ij} = \frac{A_{ij}(\epsilon D_a)_{ij}}{L_{ij}} \quad (5)$$

with D_a the local apparent diffusion coefficient. In D_a , the effect of sorption is taken into account

$$D_a = \frac{\epsilon D_p}{\epsilon + (1 - \epsilon)\rho K_d} = \frac{D_e}{\epsilon + (1 - \epsilon)\rho K_d}, \quad (6)$$

where ρ is the density of rock and K_d the local distribution coefficient. Using equations (3) and (4) for $T_{i \rightarrow j}$ can be written in form:

$$T_{i \rightarrow j} = - \sum_j \frac{\epsilon_i V_i}{w_{ij}} \log(u_{01}). \quad (7)$$

Note that D_a is equal to D_p if K_d is equal to zero in voxel i and all of its neighboring voxels and thus the two terms in equation (4) are equal (i.e., $t_s = 0$). Note also that w_{ij} cannot be used instead of b_{ij} when determining the transition probabilities since it leads to particles avoiding voxels where they can be sorbed to. In reality, it has been seen that in the rock with mineral specific distribution coefficients the elements are found more likely from places where the sorption takes place (Jokelainen et al., 2013).

2.3.1. Implementation and Parametrization of the TDRW Method

The TDRW simulations were done using a MATLAB script in which code was executed in parallel. The 3-D image from the X- μ CT analysis was first converted to matrix form with gray values assigned to the voxels. Each gray value was then linked to a given porosity, D_e and K_d , and the transition probability matrix was then determined using equation (1). The simulation was initialized by placing particles randomly into the source area next to the sample. During one simulation step two random numbers were generated. The first one was used to determine the direction of transition and the second one the transition time using equation (3). The simulation was run until a preset time was reached.

In some of the simulations, a dynamic update of K_d as a function of concentration was used. In these simulations, one thread was used to determine the particle concentration and for updating the dynamic matrix of K_d and the rest of the threads were used to determine the movement of particles and update their location information for concentration determination. Strong parallelizability of the TDRW method suffers slightly from the determination of local concentration as the particles do not move independently in these simulations. The issue was partly handled by using a short time step during which a particle can make multiple jumps. The time step was chosen at the start of simulation so that concentration does not change considerably during the step. Note that largest concentration gradients are present at the start of the simulation when there are no particles in the sample. The particle concentration in a voxel was determined by counting the amount of particles within a radius of five voxels and dividing it with the total number of voxels within the radius. The radius applied in order to decrease the total amount of particles needed for determination of local particle concentration and was chosen so that it is below the typical grain size of Grimsel granodiorite. Furthermore, the numerical effects arising were found to be negligible when testing the method with using small but representative volume of the simulation geometry. Particle concentrations were then converted to real concentrations using a ratio of particle concentration and the real concentration in the source. The K_d in the voxel was determined using the functions determined in section 2.2.1. As a maximum cesium concentration of $1 \times 10^{-3} M$ was used in the experiments by Muuri et al. (2016), the particle concentration on the face in contact with the source was determined to be less than this in order to keep the concentration range within the range of the measurement. A lower limit of the concentration range was treated by setting the K_d to the measured maximum value when the concentration was below the minimum concentration of the measurements.

The simulations this study were performed on a cubic sample with regular cells as in-diffusion and through-diffusion simulations. The parameters used in different simulations are given in Table 3. The porosity, D_e , and K_d were chosen according the previous measurements (see sections 2.1 and 2.2.1). Two types of simulation geometries were applied in the simulations: heterogeneous based on the constructed geometry and homogeneous. The homogeneous simulation geometry was used when validating the model and for comparison with the heterogeneous case using homogeneous approximation of Grimsel granodiorite. During

Table 3
The Parameters Used in Validation Simulations and in Simulations With Homogeneous and Heterogeneous Grimsel Granodiorite (GG)

Modeling case	Grid size (mm ³)	Voxel size (μm)	K _d (m ³ /kg)	ε (%)	N ₀	N _{tot}
Validation, in-diffusion	17.5 × 17.5 × 17.5	100	Various ^a	0.69	1 × 10 ⁶	4 × 10 ⁷
Validation, through diffusion	17.5 × 17.5 × 17.5	100	Various ^a	0.69	3 × 10 ⁶	3 × 10 ⁶
Validation, C-dependent K _d	17.5 × 17.5 × 17.5	100	C dependent ^b	0.69	1 × 10 ⁶	2.3 × 10 ⁷
Homogeneous GG, nonsorbing	14 × 14 × 14	80	0	0.69	1 × 10 ⁶	2 × 10 ⁶
Heterogeneous GG, nonsorbing	14 × 14 × 14	80	0	Heterogeneous ^c	1 × 10 ⁶	2 × 10 ⁶
Homogeneous GG, C dependent K _d	17.5 × 17.5 × 17.5	100	C dependent ^d	0.69	1 × 10 ⁶	1.6 × 10 ⁸
Heterogeneous GG, C-dependent K _d	14 × 14 × 14	80	C dependent ^d	Heterogeneous ^c	2.3 × 10 ⁶	1.8 × 10 ⁸
Homogeneous GG, LTD conditions	14 × 14 × 14	80	0.106	0.69	1 × 10 ⁶	2.0 × 10 ⁷
Heterogeneous GG, LTD conditions	14 × 14 × 14	80	Heterogeneous ^e	Heterogeneous ^c	1 × 10 ⁶	3.2 × 10 ⁷

Note: In all simulation D_e of 3 × 10⁻¹² m²/s was used.

^a0, 1 × 10⁻⁶, 1 × 10⁻⁵, 1 × 10⁻⁴, 1 × 10⁻³, 0.01, and 0.1 m³/kg. ^bLangmuir isotherm K_d = (αβ)/(1 + αC), α = 1 × 10⁵ and β = 1 × 10⁻⁶. ^cValues for different minerals given in Table 1. ^dFit to experimental values, see Figure 2. ^eBiotite 0.317 m³/kg, feldspar 0.106 m³/kg, and quartz 0 m³/kg.

the in-diffusion simulations, a constant particle concentration was maintained in the source by adding more particles in the simulation which were then allowed to diffuse into the sample. Due to this, the total amount of particles was considerably increased during the simulations. In through-diffusion simulations, two cells with a volume of 12.5 cm³ and a diffusion coefficient of 2 × 10⁻⁹ m²/s were assigned on opposite faces of the cubic sample. At the start of simulations, the particles were placed randomly to the first cell (source) and once the particle reached the second cell, a through diffusion time was recorded.

In the in situ test of the LTD experiment at the GTS, the initial activity concentration of ¹³⁴Cs was 540 Bq/g (Soler et al., 2015) which is equal to a molar concentration of 8.4 × 10⁻¹¹ M. As the concentration of stable cesium in Grimsel ground water is 5.3 × 10⁻⁹ M (Aksoyoglu et al., 1991), the increase in concentration of cesium due to injected ¹³⁴Cs can be neglected and simulations could be performed in a constant concentration of 5.3 × 10⁻⁹ M, and thus constant values for K_d were chosen accordingly (see Table 3 when simulating the in-diffusion profiles in in situ conditions).

2.4. Mathematical Analysis of Diffusion Simulations

Simulations validating the TDRW method and those performed in homogeneous rock were evaluated using analytical (linear K_d) and numerical (concentration-dependent K_d) solutions of the diffusion equation. These simulations were performed as in-diffusion and through-diffusion simulations. These two validation cases were selected as most of the experiments are performed using these settings. In addition to method validation, the analytical solution for the in-diffusion curve is applied in analyses of modeled in-diffusion profiles determined for Grimsel granodiorite and for estimation if the homogeneous model can explain the in-diffusion profiles from modeling with the heterogeneous sample.

2.4.1. In-Diffusion Simulations

The in-diffusion simulations were performed so that a constant concentration, C₀, of the particles was kept at one face of the cubic sample, and were allowed to diffuse through the face into the sample. The in-diffusion profiles were determined using a particle concentration as a function of distance from the face. When the elapsed time (t) was small enough, an appreciable amount of the particles did not reach the opposite face of the sample which allowed the analysis of the in-diffusion profiles by a semi-infinite approximation and the solution of the corresponding diffusion equation by Carslaw and Jaeger (1965):

$$C = C_0 - C_0 \operatorname{erf} \frac{x}{\sqrt{4D_A t}}, \tag{8}$$

where x is the distance from the intrusion surface and D_A global apparent diffusion coefficient. In the analysis, least squares fitting was done by treating the D_A as a fitting parameter. When too many particles reach the opposite face, the model breaks since particles are reflected back from there. After reaching the breaking point gradient of in-diffusion profile is zero at the opposite face since there is no flux through the face. The results from in-diffusion simulations were analyzed using least squares (equation (8)) to the simulated in-diffusion profiles by treating the D_A as a fitting parameter.

2.4.2. Through-Diffusion Simulations

In the through-diffusion simulations, a sample (length L and cross sectional area A) was placed between two particle chambers. At the start of the simulation, the particles were placed randomly into the first chamber. After a particle reached the second chamber, its arrival time was recorded in order to determine the particle flux through the sample. The diffusion and the sorption of the particles through the sample can be described by the equation:

$$\epsilon \frac{\partial C}{\partial t} + (1-\epsilon) \rho \frac{\partial C_s}{\partial t} - \nabla \cdot (\epsilon D_p \nabla C) = 0, \tag{9}$$

where C is the concentration of particles in the liquid phase, and C_s is the concentration of the particles in the solid phase. If we assume that the sample is homogeneous and the sorption is governed by a linear equilibrium isotherm and an instantaneous equilibrium between solid and liquid phases then we can describe our system with a diffusion equation in one dimension:

$$\frac{\partial C}{\partial t}(x, t) - D_A \frac{\partial^2 C}{\partial x^2}(x, t) = 0, \quad 0 < x < L, \quad t > 0. \tag{10}$$

Particle concentration in the liquid phase is continuous, and it is assumed that the concentration of the tracer is uniform in the first chamber. At the boundary $x = L$, the rate of concentration change in the first chamber and particle flux through the surface between the first chamber and sample have to be equal, and thus the boundary condition at the boundary $x = L$ can be expressed in the form:

$$V \cdot \frac{\partial C}{\partial t}(L, t) = -\epsilon A \cdot D_p \frac{\partial C}{\partial x}(L, t), \tag{11}$$

where V is volume of the chamber. In the second chamber ($x = 0$), particle concentration is kept zero, and thus the boundary condition at $x = 0$ is

$$C(0, t) = 0. \tag{12}$$

When $t = 0$ the particles are placed in the first chamber, and thus the initial condition is

$$C(x, 0) = \begin{cases} 0, & 0 \leq x < L \\ C_0, & x = L, \end{cases} \tag{13}$$

where C_0 is the initial particle concentration in the first chamber. Performing a change of variables $\tau = \frac{t D_A}{L^2}$, $\xi = \frac{x}{L}$ and $C(x, t) = C_0 u(\xi, \tau)$ leads to a dimensionless form of equation (10):

$$\frac{\partial u}{\partial \tau}(\xi, \tau) - \frac{\partial^2 u}{\partial \xi^2}(\xi, \tau) = 0, \quad 0 < \xi < 1, \quad \tau > 0 \tag{14}$$

and of the boundary and initial conditions:

$$\begin{cases} u(0, \tau) = 0 \\ \frac{\partial u}{\partial \tau}(1, \tau) = -\alpha \frac{\partial u}{\partial \xi}(1, \tau) \\ u(\xi, 0) = \begin{cases} 0, & 0 \leq \xi < 1 \\ 1, & \xi = 1, \end{cases} \end{cases} \tag{15}$$

where $\alpha = \frac{A L}{V} (\epsilon + K_d \rho)$. This equation can be solved by separating the variables. The spatial part leads to an eigenvalue problem for a trigonometric differential equation with an eigenvalue-dependent boundary condition:

$$\begin{aligned} v''(\xi) + \lambda^2 v(\xi) &= 0 \\ v(0) &= 0, \quad \alpha v'(1) = \lambda^2 v(1). \end{aligned} \tag{16}$$

The eigenvalues λ_n ($0 < \lambda_1 < \lambda_2 < \dots$) are the positive roots of the equation:

$$\lambda \tan \lambda = \alpha, \tag{17}$$

and the eigenfunctions are $v_n(\xi) = \sin \lambda_n \xi$. The functions v_n are orthogonal with respect to the scalar product:

$$\langle u, v \rangle = \int_0^1 u(\xi) v(\xi) d\xi + \frac{1}{\alpha} u(1) v(1), \tag{18}$$

and the solution can be expressed as a series expansion:

$$u(\xi, \tau) = \sum_{n=1}^{\infty} C_n e^{-\lambda_n^2 \tau} v_n(\xi). \tag{19}$$

By using the initial condition and the scalar product coefficients, C_n can be determined:

$$C_n = \frac{4 \cos \lambda_n}{2 \lambda_n + \sin 2 \lambda_n} = \frac{2 \alpha}{\sin \lambda_n (\lambda_n^2 + \alpha^2 + \alpha)}, \tag{20}$$

and the solution of the boundary value problem equations (14) and (15) becomes

$$u(\xi, \tau) = \sum_{n=1}^{\infty} \frac{2 \alpha \sin (\lambda_n \xi)}{\sin \lambda_n (\lambda_n^2 + \alpha^2 + \alpha)} e^{-\lambda_n^2 \tau}. \tag{21}$$

Finally, the solution for the concentration C can now be expressed in the form:

$$C(x, t) = C_0 \sum_{n=1}^{\infty} \frac{2 \alpha \sin (\lambda_n x / L)}{\sin \lambda_n (\lambda_n^2 + \alpha^2 + \alpha)} e^{-\frac{\lambda_n^2 D_d t}{L^2}}, \tag{22}$$

and for particle flux J_p through the surface $x = 0$ in the form:

$$J_p = \epsilon D_p \frac{\partial C}{\partial x}(0, t) = \epsilon D_p C_0 \sum_{n=1}^{\infty} \frac{2 \alpha \lambda_n}{L \sin \lambda_n (\lambda_n^2 + \alpha^2 + \alpha)} e^{-\frac{\lambda_n^2 D_d t}{L^2}}. \tag{23}$$

The results from through-diffusion simulations were analyzed by comparing simulated particle flux through the sample to one generated by analytical solution (equation (23)) using D_d determined from equation (6) and set values for local D_e , porosity and K_d (see (3)).

2.4.3. In-Diffusion Simulations With Concentration-Dependent K_d

The in-diffusion simulations with concentration-dependent K_d were performed similarly to those without concentration dependence. When sorption is governed by a nonlinear isotherm $K_d(C)$, and an instantaneous equilibrium between solid and liquid phases is assumed, C_s can be written in form:

$$C_s = K_d(C) C = : F(C), \tag{24}$$

then equation (9) gives us

$$(\epsilon + (1 - \epsilon) \rho F'(C)) \frac{\partial C}{\partial t}(x, t) - \epsilon D_p \frac{\partial^2 C}{\partial x^2}(x, t) = 0, \quad 0 < x < L, \quad t > 0. \tag{25}$$

This equation can be written in the form of equation (10) if a concentration-dependent apparent diffusion coefficient is defined:

$$D_A(C) = \frac{\epsilon D_p}{\epsilon + (1 - \epsilon) \rho (K_d(C) + K'_d(C) C)}. \tag{26}$$

Note that for the concentration independent case term $K'_d(C) C$ in equation (26) vanishes and expression for $D_A(C)$ becomes equal to equation (6). If F is "smooth enough" and F' is nonnegative and bounded, equation (25) is a quasi linear parabolic partial differential equation and it can be solved numerically (with appropriate boundary and initial conditions).

The results from in-diffusion simulations with concentration-dependent K_d were analyzed by comparing simulated in-diffusion profiles to ones from numerical solution. Equation (25) was solved numerically using

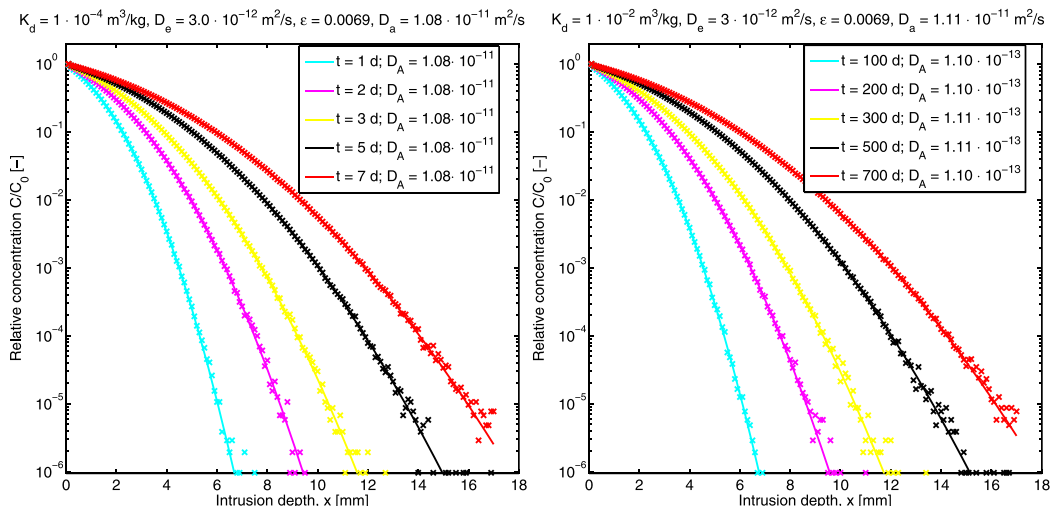


Figure 3. Validation of the TDRW method by in-diffusion simulation in a cubic homogeneous sample. The modeled in-diffusion profiles using different values for K_d (left) $0, 1 \times 10^{-6}, 1 \times 10^{-5}, 1 \times 10^{-4}, 1 \times 10^{-3}$, (right) 0.01 , and $0.1 \text{ m}^3/\text{kg}$ are in perfect agreement at all times (t) with an analytical fit by equation (8).

a pdepe-function in MATLAB and applying the same boundary and initial conditions as in the in-diffusion simulations. In the analysis, D_A determined by equation 2.4.3, set values for the local D_e and porosity, and the K_d defined by Langmuir isotherm were applied (see (3)).

3. Results

3.1. Validation of the TDRW Method With K_d Concept

Validation of the TDRW method and implemented realization for sorbing elements (see section 2.3) was done using two different homogeneous systems for which the solution can be derived analytically and one with concentration-dependent K_d for which the diffusion equation was solved numerically. Here modeled in-diffusion profiles and through-diffusion curves are compared to ones from mathematical solutions (see equations (8), (23), and (25)). Previously, Sardini et al. (2003) have validated the TDRW method using a 2-D artificial simulation grid and comparing the results to discrete-time random-walk simulations (e.g., Hunter et al., 1993). Furthermore, Voutilainen et al. (2013) have done a similar validation of the method in 3-D and also a validation in homogeneous media using rectangular and cylindrical geometries.

The results for in-diffusion and through-diffusion simulations performed to validate the TDRW method with a linear K_d are shown in Figures 3 and 4. In the in-diffusion simulations, the global apparent diffusion coefficients given by the fits differ less than 0.1% from the ones determined using equation (6) and the set values for local D_e , porosity, and K_d . Furthermore, particle fluxes through the sample from through-diffusion simulations are in perfect agreement with ones by analytical solutions (see equation (23)). These validation simulations showed that the sorption in the TDRW method was correctly implemented and that the model was constructed correctly with constant K_d .

The results for the in-diffusion simulations performed to validate the TDRW method with concentration-dependent K_d are shown in Figure 5. The in-diffusion profiles and evolution of K_d from simulations are in fair agreement with the ones by numerical solution of equation (23). In the early stage, the simulated curve overestimates slightly penetration depth and underestimates the K_d compared with the numerical solution. The difference between the curves decreases in the later stage. A small difference clearly arises from the radius used for determination of concentration. It can also be concluded that the time step for determination of concentration was small enough since its effect would hinder the in-diffusion. In general, it can be concluded that in these cases, the use of harmonic mean in equations (2) and (5) does not generate unwanted numerical bias that has been reported, e.g., by Romeu and Noetinger (1995).

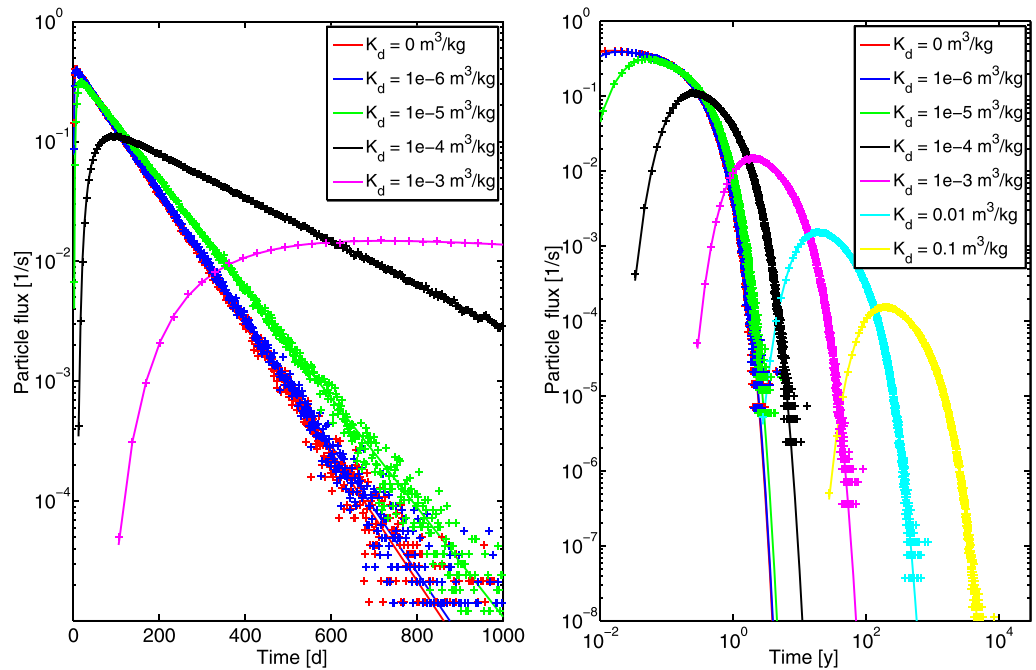


Figure 4. Validation of the TDRW method by a through-diffusion simulation in a cubic homogeneous sample. The modeled through-diffusion curves using different values for K_d (0 , 1×10^{-6} , 1×10^{-5} , 1×10^{-4} , 1×10^{-3} , 0.01 , and $0.1 \text{ m}^3/\text{kg}$) are in perfect agreement with analytical fit (equation (23)) using a set value of D_a .

3.2. Diffusion of Conservative Tracer in Heterogeneous Grimsel Granodiorite

First, the constructed 3-D mineral and porosity map was used to test how the heterogeneous porosity of Grimsel granodiorite affects the diffusion of conservative nonsorbing nuclides such as HTO. The resulting in-diffusion profiles were compared to the result from the simulation using homogeneous approximation of Grimsel granodiorite. In both cases, the in-diffusion profiles were analyzed after 2, 5, 10, 15, and 20 h from the beginning by fitting equation (8) to the profiles. The results show that the heterogeneity of porosity enhances the transport of conservative tracer by only about 1.5%. In addition, the heterogeneity does not

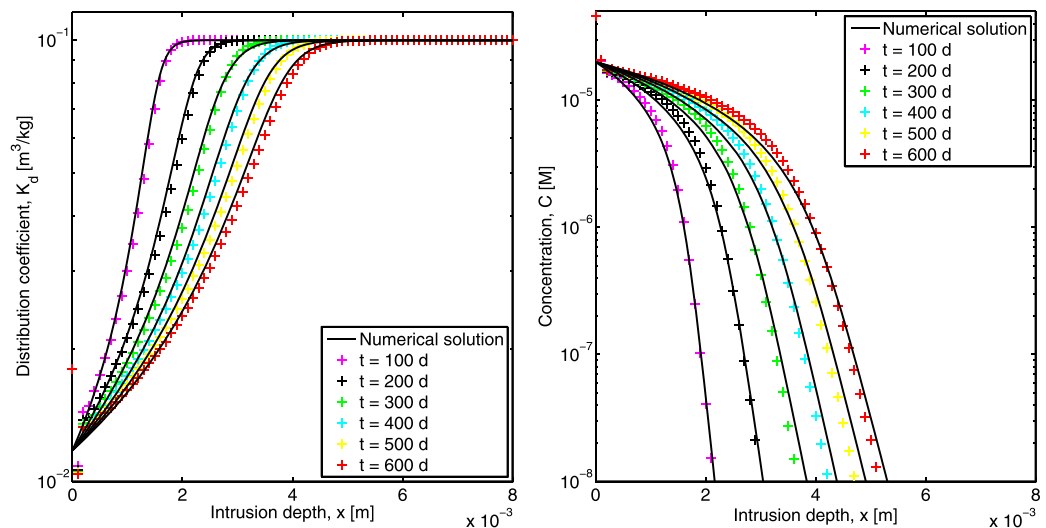


Figure 5. Validation of the TDRW method by in-diffusion simulation in a cubic sample with concentration-dependent K_d . The (left) modeled evolution of K_d and (right) in-diffusion profiles using Langmuir isotherm for $K_d(C)$ are in fair agreement at all times (t) with a numerical solution of equation (25).

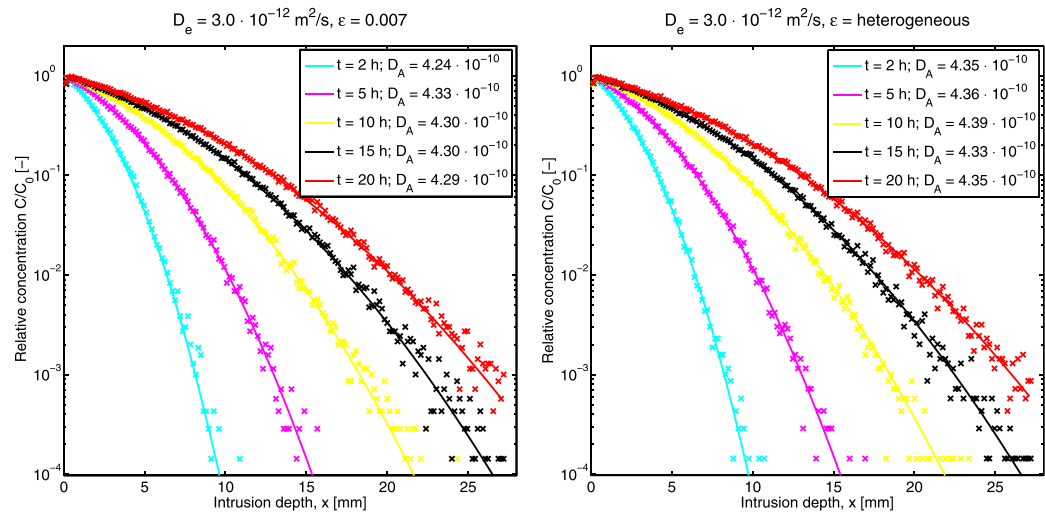


Figure 6. In-diffusion profiles of a conservative nonsorbing tracer at different times (2, 5, 10, 15, and 20 h) in Grimsel granodiorite with (left) homogeneous and (right) heterogeneous distribution of porosity. In this case, the effect of heterogeneity to the observed profile is only about 1.5%.

affect much the shape of the in-diffusion profile and they can be explained by the analytical model that was derived for homogeneous medium (see Figure 6). Furthermore, the time for analysis does not affect the analyzed D_A . It can be concluded that because the differences in the mineral specific porosities are minor, the effect of pore space heterogeneity to the in-diffusion profile is not as significant as in the previous study made for a highly altered tonalite sample (Voutilainen et al., 2013).

3.3. Diffusion and Sorption of Cesium With Concentration-Dependent K_d in Homogeneous Grimsel Granodiorite

The effect of concentration-dependent K_d to the in-diffusion profile was demonstrated using a homogenous approximation of Grimsel granodiorite. The in-diffusion profiles were analyzed after 50, 100, 150, 200, 250, 300, 350, 400, 450, 500, 550, and 600 days and the results show that the in-diffusion front proceeds with a plug-like shape (see Figure 7). The shape of these in-diffusion profiles is completely different from the one generated by simulation with linear K_d . Qualitative examination indicates that the high concentration penetrates further when using concentration-dependent K_d values than when using linear K_d values and, in contradiction, the low concentration front reaches further in case of the linear K_d values than in the

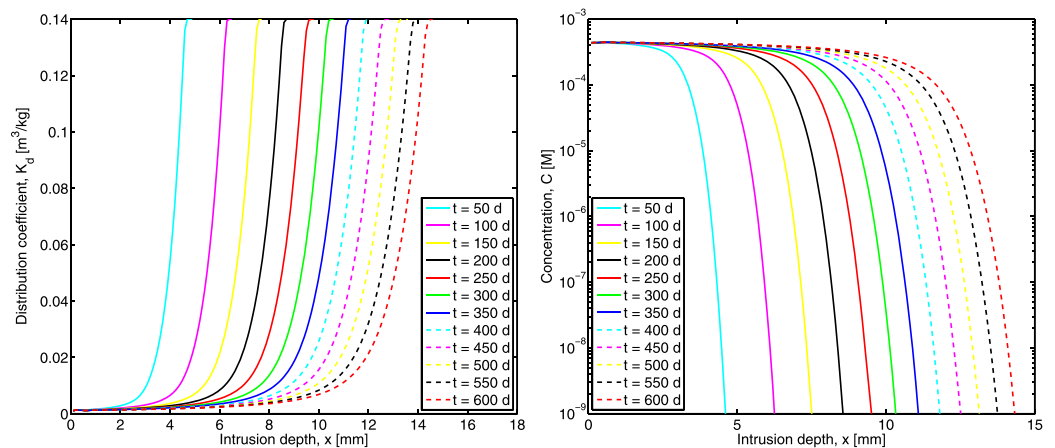


Figure 7. (right) Effect of concentration-dependent K_d to in-diffusion profiles after different times in homogenized Grimsel granodiorite is seen in the plug-like shape of the intrusion front. (left) The progression of the in-diffusion profile is in connection with the evolution of K_d as a function of intrusion depth.

concentration-dependent K_d case (see Figures 3 and 6). Furthermore, the evolution of the K_d was also analyzed as a function of intrusion depth and showed a similar front where the K_d changes relatively sharply (see Figure 7). The shape of the in-diffusion profile can be discussed further using the evolution of K_d . At the start, the K_d drops relatively rapidly near the face that is in contact with the source due to increasing concentration. The concentration cannot increase more than the source and thus the volume with nearly constant K_d and D_a is formed. This volume has a higher D_a than the one further from the source and it feeds more particles to the front where the K_d increases again. As time goes by, the front gets further from the source and it takes a longer time for the new particles to diffuse from the source to the front. This decreases the progression speed of the front with time.

In the sample with a linear K_d , the progress of the diffusion front can be described using a so-called characteristic diffusion length:

$$L_c = \sqrt{D_a^{cdl} t}, \quad (27)$$

where D_a^{cdl} is the apparent diffusion coefficient analyzed using characteristic diffusion length. Using L_c distance, where the concentration is half of the concentration from the surface in contact with source (i.e., half concentration point) global D_A can be roughly determined. As the case of a nonlinear K_d cannot be analyzed using model with linear K_d , the L_c can be used for a rough analysis of diffusion front. In this case, the characteristic diffusion lengths of 2.97, 4.26, 5.22, 6.04, 6.77, 7.42, 8.02, 8.58, 9.1, 9.6, 10.07, and 10.52 mm were determined by finding the half concentration points for different times from in-diffusion profiles shown in Figure 7. By using equation (27), these values lead to a D_a^{cdl} of $2.1 \times 10^{-12} \text{ m}^2/\text{s}$. Relatively, high value given by this analysis strengthens the qualitative examination made above about the shape and time evolution of the in-diffusion profile.

3.4. Diffusion and Sorption of Cesium With Concentration-Dependent K_d in Heterogeneous Grimsel Granodiorite

In order to demonstrate the effect of heterogeneous mineral structure in comparison to the homogeneous case presented in the previous section, similar in-diffusion simulations were performed by taking into account the heterogeneous and concentration-dependent sorption properties of Grimsel granodiorite. In addition, the simulations were performed using three different main diffusion directions to see if anisotropy affects the in-diffusion profiles. The in-diffusion profiles for all three directions were analyzed after 50, 100, 150, and 200 days. After about 200 days, the particles reached the opposite face of the sample and thus the experiment could not be considered as semi-infinite anymore.

The shape and the time evolution of the in-diffusion profiles is clearly affected by the heterogeneous sorption properties (see Figure 8). In comparison to the case of the homogeneous approximation of Grimsel granodiorite, the heterogeneous case shows faster propagation. For example, in the heterogeneous case, cesium concentration of over $1 \times 10^{-7} \text{ M}$ is found until 11–12 mm after 200 days whereas in homogeneous case such concentration only reaches 8 mm. However, the analysis for characteristic diffusion length gives average values of 1.48, 2.11, 2.65, and 3.27 mm for in-diffusion profiles shown in Figure 8. These values lead to a rough D_a^{cdl} of $5.5 \times 10^{-13} \text{ m}^2/\text{s}$ which is about a factor of four smaller than D_A from the analysis for the homogeneous case in section 3.3. The comparison shows that half of the concentration front proceeds faster in the homogenous case than in the heterogeneous case even though for small quantities are transported further in the heterogeneous case than in the homogenous case. These observations also reflect the fact that the shape of the in-diffusion profiles are not as sharp as in the homogeneous case. These differences can be explained by the presence of minerals with a lower K_d that forms pathways for faster transport than in the material with averaged K_d . The fast transport continues until a cesium particle meets a mineral phase with a high K_d . This causes fast diffusion into the matrix and a more gentle sloping in-diffusion profile than in the case of averaged K_d . The same observation applies to the shape and time evolution of K_d as a function of intrusion depth. The observation is partly self-evident because a concentration change causes a change to the local K_d . However, this strengthens the conclusion that in the case of matrix with highly sorptive minerals heterogeneity has a strong effect to the transport of cesium. Small waves in the concentration and K_d curves are caused by local variations due to heterogeneity and weak orientation of the biotite causes small differences to in-diffusion profiles determined using different main diffusion directions.

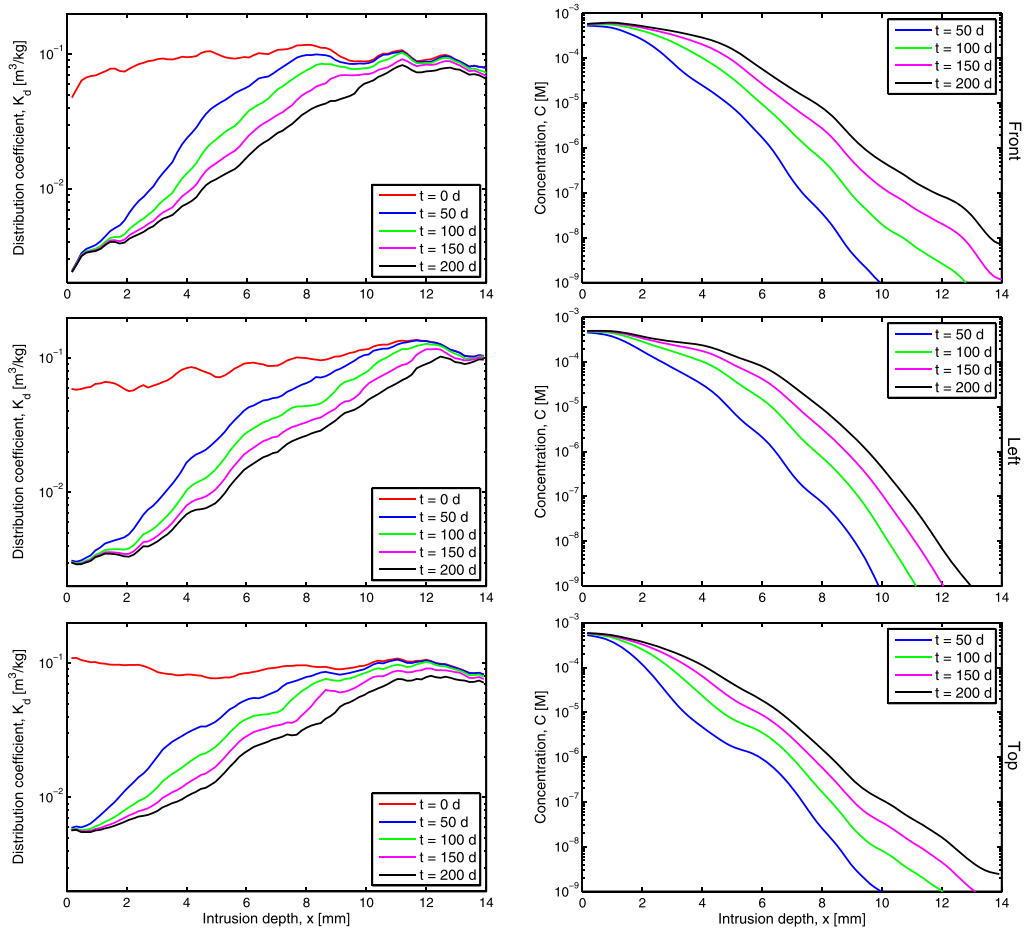


Figure 8. (left) The heterogeneity of Grimsel granodiorite and concentration-dependent K_d affect the time evolution of the volumetric mean K_d of cesium as a function of distance from the injection face and (right) to the in-diffusion profiles of cesium compared to cases with a homogeneous sample and linear K_d (see Figures 3 and 7). Weak orientation of the sample causes small differences to result between main diffusion directions from (top) front, (middle) left, and (bottom) top.

The conclusions listed above can be confirmed by looking at the spatial concentration distribution inside the sample during the simulation and by comparing the distribution to the location of different minerals (see Figure 9). Particle concentration distribution reflects the mineral structure of the area: quartz areas show low particle concentration due to negligible K_d , feldspar areas show intermediate particle concentration due to moderate K_d , and biotite area has a high particle concentration due to higher K_d (see Figures 9a and 9d). The concentration decreases when going further from the source but the distribution still reflects the mineral structure. The modeled distributions presented in Figures 9b and 9c are similar to distributions visualized by autoradiography in earlier study for Grimsel granodiorite (Jokelainen et al., 2013). Furthermore, nearly similar cesium concentration distributions have been determined in in-diffusion experiments using Äspö and Olkiluoto rock samples with the same main minerals but with relatively high variation in their quantities (Nilsson et al., 2010; Puukko, 2014; Widestrand et al., 2007). In these studies, heterogeneity of the mineral structure has been mentioned as a possible explanation for the observed spatial concentration distributions but it has not been possible to reproduce them by using available modeling tools.

3.5. Effect of Heterogeneity in In Situ Conditions (LTD Experiment)

In the previous sections, a relatively large concentration range of cesium has been used to demonstrate the ultimate effect of the concentration-dependent K_d . In the in situ LTD experiment, the effect of concentration to K_d can be neglected. The results of simulations identical to in situ conditions in LTD experiment were analyzed after 100, 200, 300, 400, 500, and 600 days and they show that the heterogeneity affects significantly

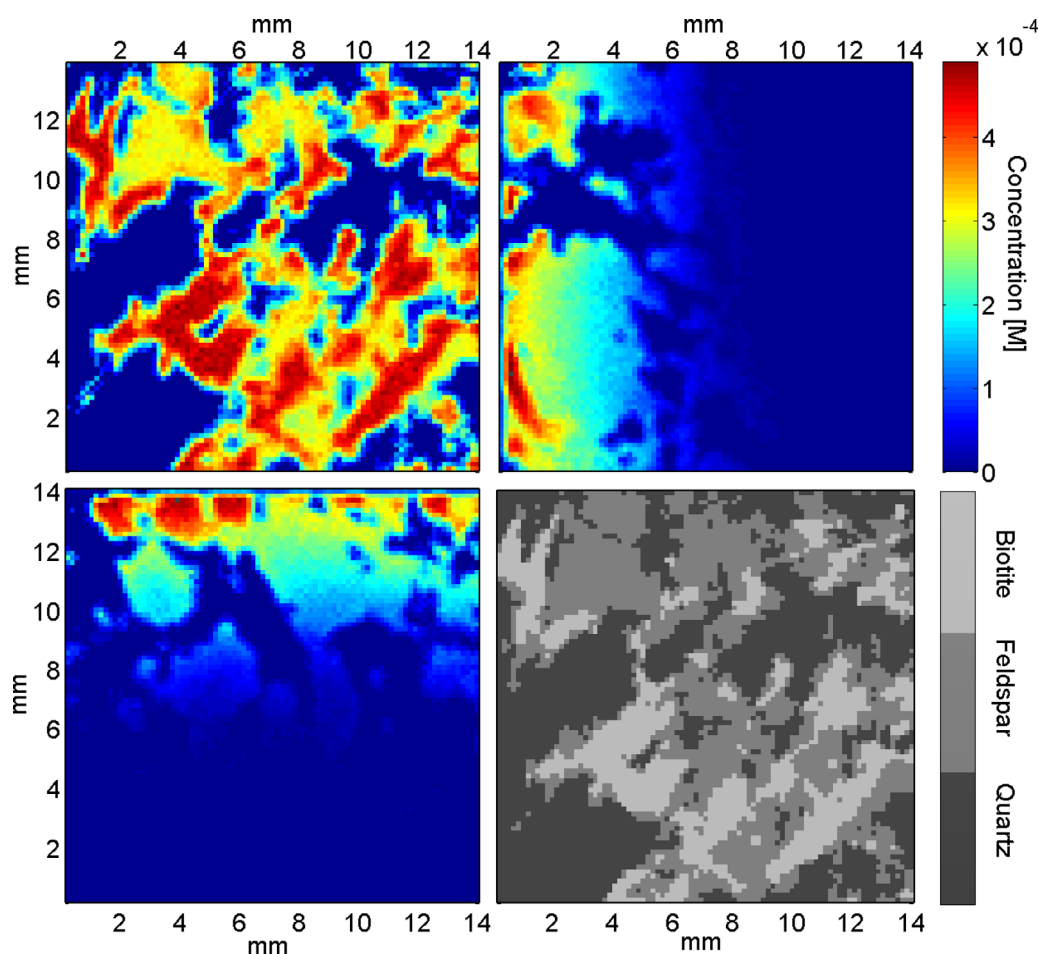


Figure 9. Illustration of (left top) the spatial concentration distribution of cesium (right bottom) on mineral surface and spatial concentration distributions inside the sample in (right top) vertical direction (8.0 mm) and (left bottom) horizontal direction (4.2 mm). The mineral surface shows the location of quartz (dark gray), feldspar (gray), and biotite (light gray), and they correspond to low, mediocre, and high cesium concentrations, respectively.

the shape of the in-diffusion profile (see Figure 10). Furthermore, the heterogeneity increases the transport of cesium by diffusion so that the D_A analyzed by equation (8) increases from 1.1×10^{-14} to about 2.5×10^{-14} . Note also that here the fitting was done for the early part of the in-diffusion profile which leads to the underestimation of diffusion length in heterogeneous rock. It can be seen that the fit fails to explain the late part of the in-diffusion profile which extends further than the fit to the early part predicts. Similar challenges were faced when analyzing the in-diffusion profiles from the LTD experiment and the analysis could not be performed using homogeneous models (Jokelainen et al., 2013; Soler et al., 2015; Tachi et al., 2015). The overall shape of the profiles is similar but modeled ones do not extend as far as the ones from the LTD experiment. This is due to the K_d values that were determined for crushed rock which overestimate the K_d of intact rock as the crushing increases the specific surface area of the rock (Muuri et al., 2016; Tachi et al., 2015). In a previous study by Tachi et al. (2015), it was shown that this effect depends on the grain size used in batch sorption experiments and that the K_d of cesium was overestimated for about 1 order of magnitude when using a grain size of 0.1–0.5 mm. Furthermore, the modeled in-diffusion profiles do not take into account the effect of the BDZ (borehole disturbed zone) because the sample used in this study did not contain any surface disturbance. In-diffusion profiles of cesium with a similar shape have also been observed in experiments performed in crystalline rock samples from Äspö (Johansson et al., 1998). They used a dual-component model for explaining the in-diffusion profiles and justified its application by the heterogeneity of the crystalline rock. These experiments were performed in fine grained Äspö diorite which has a relatively similar mineral content to that of Grimsel granodiorite. However, the ionic strength and thus

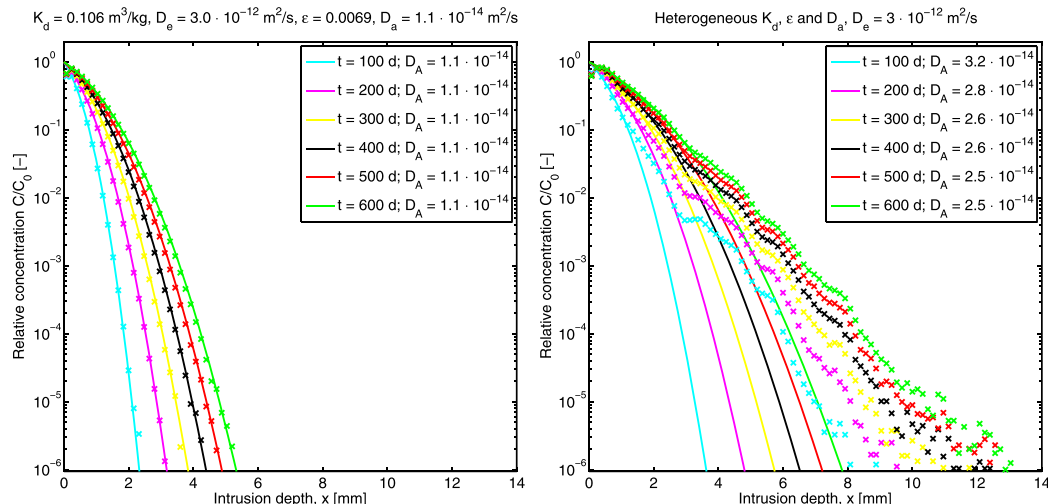


Figure 10. In-diffusion profiles of cesium at different times (100, 200, 300, 400, 500, and 600 days) in conditions of the LTD experiment performed in the GTS with a (left) homogeneous and (right) heterogeneous mineral structure. In this case, the heterogeneity affects significantly the shape of the profile and increases the rate of transport by diffusion compared to the homogeneous rock.

the amount of competing ions for sorption is higher in Äspö groundwater than in Grimsel. The results between these experiments are not fully comparable but the agreement between the in-diffusion profiles builds confidence on the results as the main focus here has been to determine the effect of heterogeneity of mineral and pore structure on the transport of cesium.

The maximum concentration of cesium in the conditions of the spent nuclear fuel repository can be estimated using the following parameters from a repository being built in Olkiluoto Finland. In the current design, the volume of a canister is 3.2 m³ and it contains 16 spent fuel assemblies with a total weight of 2,880 kg of spent nuclear fuel (Posiva, 2012). It can be determined that about 500 g/tU of Cs-135 is left in the spent nuclear fuel after 30 years of storage prior to disposal (Smith et al., 2007) and that there is about 1,630 g/MTHM of inactive Cs-133 in it (OECD, 2011). Furthermore, it has been estimated that cesium has an instant release fraction of about 2% (Zwicky et al., 2011). These values lead to an estimation that under these conditions near a damaged canister, the concentration of cesium would be about 1×10^{-4} M. In comparison, the concentration of cesium in Olkiluoto groundwater varies from 2×10^{-9} to 1×10^{-6} M (Hellä et al., 2014). It can be concluded that in principle these values are in agreement with the ones used in section 3.4 and thus one could expect similar in-diffusion profiles of cesium as in Figure 8 in the case a canister is damaged during emplacement. In this study, the focus has been on the effect of micrometer scale heterogeneity to the transport in centimeter scale whereas in the safety analysis of a geological disposal of spent nuclear fuel the main interest is on the transport properties on the scale of tens and hundreds of meters. However, it is needed to fully understand micrometer scale process in order to be able to evaluate the transport to larger scale.

4. Discussion and Future Prospects

The TDRW method was successfully validated in the cases of linear K_d and concentration-dependent K_d and multiple nonlinear feedback effects arising from the heterogeneity of Grimsel granodiorite and where concentration dependence of K_d was observed. However, there are a couple of strongly case-dependent parameters remaining that may cause some numerical stability problems if not properly handled. First, the radius used to determine the local concentration is needed in order to decrease calculation time and memory usage. However, it has to be carefully selected as it might cause numerical artifacts. In the case of a heterogeneous sample, the grain size has also to be taken into account. Second, stepwise determination saves some advances regarding parallelizability in respect to traditional methods. However, the time step has to

be small enough so that concentration does not change considerably within each time step. If these approximations are too large, the results would differ considerably from the real ones.

Furthermore, a considerable amount of experimental work has to be performed before the TDRW method can be applied in this extent. However, there are experimental and practical issues regarding structure characterization that might cause some defects to the rock structure. Typically compromises have to be made regarding image resolution and sample size when using X- μ CT data. Here the aim was to study effects of micrometer scale heterogeneities on centimeter scale transport and the compromise was made accordingly. Furthermore, the artifacts in X- μ CT (e.g., beam hardening, ring artifacts image noise, partial-volume effect, and starburst artifact) might cause some problems for constructing the simulation geometry. Fortunately, commercially available image reconstruction programs include features that reduce the effect of these artifacts. In our case, the main issue in construction of a simulation geometry was that X-ray attenuation coefficients of plagioclase and K-feldspar overlapped and thus they had to be treated as one mineral phase. Fortunately, their transport properties are rather similar compared to that of biotite and quartz, and thus the error due to this assumption can be considered to be negligible. Furthermore, the effect of heterogeneity in in-diffusion simulations is mainly arising from the difference between the K_d of quartz and biotite. As particles can diffuse more freely in quartz grains than in biotite, rapid diffusion takes place in quartz grains and when a particle meets a biotite grain it gets sorbed and diffusion hindered.

Looking beyond the results obtained in this study, the TDRW method and results from structure characterization results could (i) be further developed by constructing a more accurate porosity distribution of the sample in 3-D by using 2-D spatial porosity distribution including fractures and fissures from C-14-PMMA autoradiography and appropriate image processing algorithms, (ii) be used to model other phenomena such as advection in fractured rock, (iii) be used to model the transport of elements with changing species according to chemical conditions, and (iv) support the upscaling from micrometer scale to the meter scale that is more relevant for the safety analysis of spent nuclear fuel repositories. In principle, with the developments listed above, the TDRW method could also be used to model advection and diffusion of elements in a flowing fracture adjacent to rock matrix with potential structural evolution (e.g., dissolution/precipitation processes) due to water-rock interactions. On a larger scale, the heterogeneity of crystalline rock consists of different rock types, fractures, and shear zones. In principle, it is possible to include such heterogeneities into the TDRW method. However, as pressure gradients and water conducting shear zones play important roles in larger scales, a method development on these issues and structure characterization for large scale is also required.

5. Conclusions

The effect of the micrometer scale heterogeneities of Grimsel granodiorite was studied to understand the transport of cesium in centimeter scale. In order to do this, the TDRW method was improved by implementing nonlinear sorption using a concentration-dependent K_d . The TDRW method was successfully validated using in-diffusion and through-diffusion simulations in case of a linear K_d using the analytical solutions of diffusion equation and in case of a concentration-dependent K_d using the numerical solution of diffusion equation. Furthermore, the results of X- μ CT, C-14-PMMA autoradiography, and conventional batch sorption experiments were applied for constructing the 3-D mineral map of Grimsel granodiorite with spatial information on the porosity and K_d of cesium. It can be summarized that heterogeneity of Grimsel granodiorite on micrometer scale: (i) does not affect considerably the diffusion of conservative tracers such as HTO due to the homogeneously distributed porosity and (ii) enhances the diffusion of cesium significantly at centimeter scale in comparison to the homogeneous approximation of the medium because of the large differences in K_d of cesium on different minerals.

In general, acquiring the realistic micrometer scale structure of the rock and applying it in TDRW modeling, framework offers new insights for understanding previously observed experimental results and diffusion behavior of cesium. The in-diffusion profiles and the heterogeneous spatial concentration distribution of cesium determined in this work were similar to the ones from previous LTD and laboratory experiments that were performed in crystalline rock. More importantly, as it was shown that heterogeneity affects significantly the diffusion of cesium, it cannot be neglected when analyzing and interpreting such experiments. In

this study, cesium was used as an example but it can be expected that similar conclusions could be drawn for other sorbing elements, especially if there is preferential sorption to at least one of the minerals in the rock.

Acknowledgements

Funding by Finnish Research programme on Nuclear waste Management is gratefully acknowledged.

References

- Aksoyoglu, S., Bajo, C., & Mantovani, M. (1991). *Batch sorption experiments with iodine, bromine, strontium and cesium on Grimsel mylonite* (NTB Rep. 91-06). Wettingen, Switzerland: Nagra.
- Amano, H., Matsunaga, T., Nagao, S., Hanzawa, Y., Watanabe, M., Ueno, T., & Onuma, Y. (1999). The transfer capability of long-lived Chernobyl radionuclides from surface soil to river water in dissolved forms. *Organic Geochemistry*, *30*, 437–442.
- Berkowitz, B., Scher, H., & Silliman, S. (2000). Anomalous transport in laboratory-scale, heterogeneous porous media. *Water Resources Research*, *36*(1), 149–158.
- Blessent, D., Therrien, R., & Gable, C. W. (2011). Large-scale numerical simulation of groundwater flow and solute transport in discretely-fractured crystalline bedrock. *Advances in Water Resources*, *34*(12), 1539–1552.
- Byegård, J., Johansson, H., Skälberg, M., & Tullborg, E.-L. (1995). *The interaction of sorbing and non-sorbing tracers with different Äspö rock types. Sorption and diffusion experiments in the laboratory scale* (Tech. Rep. TR-98-18). Stockholm, Sweden: Svensk kärnbränslehantering AB.
- Carlsaw, H., & Jaeger, J. (1965). *Conduction of heat in solids*. Oxford, UK: Clarendon Press.
- Cnudde, V., & Boone, M. (2013). High-resolution X-ray computed tomography in geosciences: A review of the current technology and applications. *Earth Science Reviews*, *123*, 1–17.
- Cvetkovic, V., Cheng, H., Widestrand, H., Byegård, J., Winberg, A., & Andersson, P. (2007). Sorbing tracer experiments in a crystalline rock fracture at Äspö (Sweden): 2. Transport model and effective parameter estimation. *Water Resources Research*, *43*, W11421. <https://doi.org/10.1029/2006WR005278>
- Cvetkovic, V., Cheng, H., Widestrand, H., Byegård, J., Winberg, A., & Andersson, P. (2010). Significance of fracture rim zone heterogeneity for tracer transport in crystalline rock. *Water Resources Research*, *46*, W03504. <https://doi.org/10.1029/2009WR007755>
- Cvetkovic, V., Selroos, J.-O., & Cheng, H. (1999). Transport of reactive tracers in rock fractures. *Journal of Fluid Mechanics*, *378*, 335–356.
- Delay, F., & Porel, G. (2003). Inverse modeling in the time domain for solving diffusion in a heterogeneous rock matrix. *Geophysical Research Letters*, *30*(3), 1147. <https://doi.org/10.1029/2002GL016428>
- Delay, F., Porel, G., & Sardini, P. (2002). Modelling diffusion in a heterogeneous rock matrix with a time-domain Lagrangian method and an inversion procedure. *Comptes Rendus Geoscience*, *334*(13), 967–973.
- Dentz, M., Gouze, P., Russian, A., Dweik, J., & Delay, F. (2012). Diffusion and trapping in heterogeneous media: An inhomogeneous continuous time random walk approach. *Advances in Water Resources*, *15*(1), 13–22.
- Dentz, M., Le Borgne, T., Englert, A., & Bijeljic, B. (2011). Mixing, spreading and reaction in heterogeneous media: A brief review. *Journal of Contaminant Hydrology*, *120–121*, 1–17.
- Flügge, J., Stockmann, M., Schneider, A., & Noseck, U. (2013). The impact of climate transitions on the radionuclide transport through a sedimentary aquifer. In J. Cobbing, S. Adams, I. Dennis, & K. Riemann (Eds.), *Assessing and managing ground water in different environments* (pp. 147–165). Boca Raton, FL: CRC Press.
- Forsyth, D. A., & Ponce, J. (2002). *Computer vision: A modern approach*. Upper Saddle River, NJ: Prentice Hall.
- Fuseseis, F., Xiao, X., Schrank, C., & De Carlo, F. (2014). A brief guide to synchrotron radiation-based microtomography in (structural) geology and rock mechanics. *Journal of Structural Geology*, *65*, 1–16.
- Ganapathysubramanian, B., & Zabarav, N. (2007). Modeling diffusion in random heterogeneous media: Data-driven models, stochastic collocation and the variational multiscale method. *Journal of Computational Physics*, *226*(1), 326–353.
- Genty, A., & Pot, V. (2014). Numerical calculation of effective diffusion in unsaturated porous media by the TRT lattice Boltzmann method. *Transport in Porous Media*, *105*(2), 139–410.
- Gjetvaj, F., Russian, A., Gouze, P., & Dentz, M. (2015). Dual control of flow field heterogeneity and immobile porosity on non-Fickian transport in Berea sandstone. *Water Resources Research*, *51*, 8273–8293. <https://doi.org/10.1002/2015WR017645>
- Glaus, M., Aertsens, M., Maes, N., Van Laer, L., & Van Loon, L. R. (2015). Treatment of boundary conditions in through-diffusion: A case study of $^{85}\text{Sr}^{2+}$ diffusion in compacted illite. *Journal of Contaminant Hydrology*, *177–178*, 239–248.
- Gonzalez, R., & Woods, R. (2002). *Digital image processing*. Upper Saddle River, NJ: Prentice Hall.
- Gouze, P., Melean, Y., Le Borgne, T., Dentz, M., & Carrera, J. (2008). Non-Fickian dispersion in porous media explained by heterogeneous microscale matrix diffusion. *Water Resources Research*, *44*, W11416. <https://doi.org/10.1029/2007WR006690>
- Hadermann, J., & Heer, W. (1996). The Grimsel (Switzerland) migration experiment: Integrating field experiments, laboratory investigations and modelling. *Journal of Contaminant Hydrology*, *21*(1–4), 87–100.
- Hartikainen, J., Hartikainen, K., Hautojärvi, A., Kuoppamäki, K., & Timonen, J. (1996). *Helium gas methods for rock characteristics and matrix diffusion* (Posiva Rep. 96-22). Eurajoki, Finland: Posiva Oy.
- Hellä, P., Pitkänen, P., Löfman, J., Partamies, S., Vuorinen, U., & Wersin, P. (2014). *Safety case for the disposal of spent nuclear fuel at Olkiluoto: Definition of reference and bounding groundwaters, buffer and backfill porewaters* (Posiva Rep. 2014-04). Eurajoki, Finland: Posiva Oy.
- Hellmuth, K.-H., Lukkarinen, S., & Siitari-Kauppi, M. (1994). Rock matrix studies with carbon-14-polymethylmethacrylate (PMMA): Method development and applications. *Isotopes in Environmental and Health Studies*, *30*(1), 47–60.
- Hellmuth, K.-H., Siitari-Kauppi, M., & Lindberg, A. (1993). Study of porosity and migration pathways in crystalline rock by impregnation with ^{14}C -polymethylmethacrylate. *Journal of Contaminant Hydrology*, *13*(1–4), 403–418.
- Hirose, K. (2012). 2011 Fukushima Dai-ichi nuclear power plant accident: Summary of regional radioactive deposition monitoring results. *Journal of Environmental Radioactivity*, *111*, 13–17.
- Hunter, J., Craig, P., & Phillips, H. (1993). On the use of random walk models with spatially variable diffusivity. *Journal of Computational Physics*, *106*(2), 366–376.
- IAEA. (2008). *Estimation of global inventories of radioactive waste and other radioactive materials* (Tech. Rep. IAEA-TECDOC-1591). Vienna, Austria: Author.
- Ikonen, J., Sardini, P., Jokelainen, L., Siitari-Kauppi, M., Martin, A., & Eikenberg, J. (2016a). The tritiated water and iodine migration in situ in Grimsel granodiorite. Part I: Determination of the diffusion profiles. *Journal of Radioanalytical and Nuclear Chemistry*, *310*(3), 1041–1048.
- Ikonen, J., Sardini, P., Siitari-Kauppi, M., & Martin, A. (2017). In situ migration of tritiated water and iodine in Grimsel granodiorite. Part II: Assessment of the diffusion coefficients by TDD modelling. *Journal of Radioanalytical and Nuclear Chemistry*, *311*(1), 339–348.

- Ikonen, J., Voutilainen, M., Söderlund, M., Jokelainen, L., Siitari-Kauppi, M., & Martin, A. (2016b). Sorption and diffusion of selenium oxyanions in granitic rocks. *Journal of Contaminant Hydrology*, *192*, 203–211.
- Ittner, T., Torstenfeit, B., & Allard, B. B. (1990). Diffusion of strontium, technetium, iodine and cesium in granitic rock. *Radiochimica Acta*, *49*, 101–106.
- Jeong, N., Choi, D., & Lin, C.-L. (2008). Estimation of thermal and mass diffusivity in a porous medium of complex structure using a lattice Boltzmann method. *International Journal of Heat and Mass Transfer*, *51*(15–16), 3913–3923.
- Johansson, H., Siitari-Kauppi, M., Skälberg, M., & Tullborg, E.-L. (1998). Diffusion pathways in crystalline rock—Examples from Äspö-diorite and fine-grained granite. *Journal of Contaminant Hydrology*, *35*(1–3), 41–53.
- Jokelainen, L., Meski, T., Lindberg, A., Soler, J., Siitari-Kauppi, M., Martin, A., & Eikenberg, J. (2013). The determination of ^{134}Cs and ^{22}Na diffusion profiles in granodiorite using gamma spectroscopy. *Journal of Radioanalytical and Nuclear Chemistry*, *295*, 2153–2161.
- Kekäläinen, P., Voutilainen, A., Poteri, M., Hölltö, P., Hautojärvi, A., & Timonen, J. (2011). Solutions to and validation of matrix-diffusion models. *Transport in Porous Media*, *87*(1), 125–149.
- Kelokaski, M., Siitari-Kauppi, M., Sardini, P., Möri, A., & Hellmuth, K.-H. (2006). Characterisation of pore space geometry by ^{14}C -PMMA impregnation—Development work for in situ studies. *Journal of Geochemical Exploration*, *90*(1–2), 45–52.
- Klepikova, M. V., Borgne, T. L., Bour, O., Dentz, M., Hochreutener, R., & Lavenant, N. (2016). Heat as a tracer for understanding transport processes in fractured media: Theory and field assessment from multiscale thermal push-pull tracer tests. *Water Resources Research*, *52*, 5442–5457. <https://doi.org/10.1002/2016WR018789>
- Kuva, J., Voutilainen, M., Kekäläinen, P., Siitari-Kauppi, M., Sammaljärvi, J., Timonen, J., & Koskinen, L. (2016). Gas phase measurements of matrix diffusion in rock samples from Olkiluoto bedrock, Finland. *Transport in Porous Media*, *115*(1), 1–20.
- Kuva, J., Voutilainen, M., Kekäläinen, P., Siitari-Kauppi, M., Timonen, J., & Koskinen, L. (2015). Gas phase measurements of porosity, diffusion coefficient, and permeability in rock samples from Olkiluoto bedrock, Finland. *Transport in Porous Media*, *107*(1), 187–204.
- Kyllönen, J., Hakanen, M., Lindberg, A., Harjula, R., Vehkamäki, M., & Lehto, J. (2014). Modeling of cesium sorption on biotite using cation exchange selectivity coefficients. *Radiochimica Acta*, *102*(10), 919–929.
- Mäder, U. K., Fierz, T. T., Frieg, B., Eikenberg, J., Rüthi, M., Albinsson, Y., . . . Stille, P. (2006). Interaction of hyperalkaline fluid with fractured rock: Field and laboratory experiments of the HPF project (Grimsel Test Site, Switzerland). *Journal of Geochemical Exploration*, *90*, 68–94.
- McCarthy, J. (1993). Continuous-time random walks on random media. *Journal of Physics A: Mathematical and General*, *26*, 2495–2503.
- Mettier, R., Kosakowski, G., & Kolditz, O. (2006). Influence of small-scale heterogeneities on contaminant transport in fractured crystalline rock. *Ground Water*, *44*(5), 687–696.
- Möri, A., Schild, M., Siegesmund, S., Vollbrecht, A., Adler, M., Mazurek, M., . . . Alexander, W. (2003). *The Nagra-JNC in situ study of safety relevant radionuclide retardation in fractured crystalline rock IV: The in situ study of matrix porosity in the vicinity of a water-conducting fracture* (NTB Rep. 00–08). Wettingen, Switzerland: Nagra.
- Muuri, E., Ikonen, J., Matara-Aho, M., Lindberg, A., Holgersson, S., Voutilainen, M., . . . Martin, A. (2016). Behavior of Cs in Grimsel granodiorite: Sorption on main minerals and crushed rock. *Radiochimica Acta*, *104*(8), 575–582.
- Muuri, E., Siitari-Kauppi, M., Matara-Aho, M., Ikonen, J., Lindberg, A., Qian, L., & Koskinen, L. (2017). Cesium sorption and diffusion on crystalline rock: Olkiluoto case study. *Journal of Radioanalytical and Nuclear Chemistry*, *311*(1), 439–446.
- Nilsson, K., Byegård, J., Selner, E., Widestrand, H., Höglund, S., & Gustafsson, E. (2010). *Äspö hard rock laboratory long term sorption diffusion experiment (LTDE-SD): Results from rock sample analyses and modelling* (Tech. Rep. SKB R-10–68). Stockholm, Sweden: Svensk kärnbränslehantering AB.
- Noetinger, B., & Estebenet, T. (2000). Up-scaling of double porosity fractured media using continuous-time random walks methods. *Transport in Porous Media*, *39*, 315–337.
- Noetinger, B., Roubinet, D., Russian, A., Le Borgne, T., Delay, F., Dentz, M., . . . Gouze, P. (2016). Random walk methods for modeling hydrodynamic transport in porous and fractured media from pore to reservoir scale. *Transport in Porous Media*, *115*(2), 345–385.
- Noseck, U., Britz, S., Flügge, J., Mönig, J., Brendler, V., & Stockmann, M. (2014). *New methodology for realistic integration of sorption processes safety assessments*. Paper presented at the WM2014 Conference Proceedings, Phoenix, AZ.
- OECD. (2011). *Spent nuclear fuel assay data for isotopic validation: State-of-the-art report* (Tech. Rep. NEA/NSC/WPNC/DOC(2011)5). Paris, France: Author.
- Ohta, T., Mahara, Y., Kubota, T., Fukutani, S., Fujiwara, K., Takamiya, K., . . . Igarashi, T. (2012). Prediction of groundwater contamination with ^{137}Cs and ^{131}I from the Fukushima nuclear accident in the Kanto district. *Journal of Environmental Radioactivity*, *111*, 38–41.
- Pinnioja, S., Jaakkola, T., & Miettinen, J. K. (1983). Comparison of batch and autoradiographic methods in sorption studies of radionuclides in rock and mineral samples. *Scientific Basis for Nuclear Waste Management VII, MRS Proceedings*, *26*, 1099–1105.
- Posiva. (2012). *Safety case for the disposal of spent nuclear fuel at Olkiluoto—Description of the disposal system 2012* (Posiva Rep. 2012-05). Eurajoki, Finland: Posiva Oy.
- Posiva. (2013). *Safety case for the disposal of spent nuclear fuel at Olkiluoto—Models and data for the repository system 2012* (Posiva Rep. 2013-01). Eurajoki, Finland: Posiva Oy.
- Puukko, E. (2014). *Sorption of cesium on intact rock* (Working Rep. 2014-13). Eurajoki, Finland: Posiva Oy.
- Robinet, J., Sardini, P., Coelho, D., Parneix, J., Prêt, D., Sammartino, S., . . . Altmann, S. (2012). Effects of mineral distribution at mesoscopic scale on solute diffusion in a clay-rich rock: Example of the Callovo-Oxfordian mudstone (Bure, France). *Water Resources Research*, *48*, W05554. <https://doi.org/10.1029/2011WR011352>
- Robinet, J., Sardini, P., Delay, F., & Hellmuth, K.-H. (2008). The effect of rock matrix heterogeneities near fracture walls on the residence time distribution (RTD) of solutes. *Transport in Porous Media*, *72*(3), 393–408.
- Romeu, R. K., & Noetinger, B. (1995). Calculation of internodal transmissivities in finite difference models of flow in heterogeneous porous media. *Water Resources Research*, *31*(4), 943–959.
- Russian, A., Dentz, M., & Gouze, P. (2016). Time Domain Random Walks for hydrodynamic transport in heterogeneous media. *Water Resources Research*, *52*, 3309–3323. <https://doi.org/10.1002/2015WR018511>
- Sammaljärvi, J., Jokelainen, L., Ikonen, J., & Siitari-Kauppi, M. (2012). Free radical polymerisation of MMA with thermal initiator in brick and Grimsel granodiorite. *Engineering Geology*, *135–136*, 52–59.
- Sammaljärvi, J., Shroff Rama, M., Ikonen, J., Muuri, E., Hellmuth, K.-H., & Siitari-Kauppi, M. (2016). Free radical polymerisation of methacrylates with thermal initiator in clay rock. *Engineering Geology*, *210*, 70–83.
- Sanada, Y., Matsunaga, T., Yanase, N., Nagao, S., Amano, H., Takada, H., & Tkachenko, Y. (2002). Accumulation and potential dissolution of Chernobyl-derived radionuclides in river bottom sediment. *Applied Radiation and Isotopes*, *56*(5), 751–760.
- Sardini, P., Caner, L., Mossler, P., Mazurier, A., Hellmuth, K.-H., Graham, R. C., . . . Siitari-Kauppi, M. (2015). Calibration of digital autoradiograph technique for quantifying rock porosity using ^{14}C -PMMA method. *Journal of Radioanalytical and Nuclear Chemistry*, *303*, 11–23.

- Sardini, P., Delay, F., Hellmuth, K.-H., Porel, G., & Oila, E. (2003). Interpretation of out-diffusion experiments on crystalline rocks using random walk modeling. *Journal of Contaminant Hydrology*, *61*(1–4), 339–350.
- Sardini, P., Robinet, J., Siitari-Kauppi, M., Delay, F., & Hellmuth, K.-H. (2007). Direct simulation of heterogeneous diffusion and inversion procedure applied to an out-diffusion experiment. Test case of Palmottu granite. *Journal of Contaminant Hydrology*, *93*(1–4), 21–37.
- Sardini, P., Siitari-Kauppi, M., Beaufort, D., & Hellmuth, K.-H. (2006). On the connected porosity of mineral aggregates in crystalline rocks. *American Mineralogist*, *91*(7), 1069–1080.
- Sasaki, T., Terakado, Y., Kobayashi, T., Takagi, I., & Moriyama, H. (2007). Analysis of sorption behavior of cesium ion on mineral components of granite. *Journal of Nuclear Science and Technology*, *44*(4), 641–648.
- Sasov, A., & Van Dyck, D. (1998). Desktop X-ray microscopy and microtomography. *Journal of Microscopy*, *191*(2), 113–220.
- Schild, M., Siegesmund, S., Vollbrecht, A., & Mazurek, M. (2001). Characterization of granite matrix porosity and pore-space geometry by in situ and laboratory methods. *Geophysical Journal International*, *146*, 111–125.
- Schladitz, K. (2011). Quantitative micro-CT. *Journal of Microscopy*, *243*(2), 111–117.
- Siitari-Kauppi, M. (2002). *Development of ¹⁴C-polymethylmethacrylate method for the characterisation of low porosity media: Application to rocks in geological barriers of nuclear waste storage, Report series in radiochemistry 17*. Helsinki, Finland: University of Helsinki.
- Skagius, K., & Neretnieks, I. (1988). Measurements of cesium and strontium diffusion in biotite gneiss. *Water Resources Research*, *24*(1), 75–84.
- Smith, P., Nordman, H., Pastina, B., Snellman, M., Hjerpe, T., & Johnson, L. (2007). *Safety assessment for a KBS-3H spent nuclear fuel repository at Olkiluoto: Radionuclide transport report* (Posiva Rep. 2007-07). Eurajoki, Finland: Posiva Oy.
- Soler, J., Landa, J., Havlova, V., Tachi, Y., Ebina, T., Sardini, P., . . . Martin, A. J. (2014). Modeling of an in-situ diffusion experiment in granite at the Grimsel Test Site. *Scientific Basis for Nuclear Waste Management XXXVII, MRS Proceedings*, *1665*, 85–91.
- Soler, J. M., Landa, J., Havlova, V., Tachi, Y., Ebina, T., Sardini, P., . . . Martin, A. J. (2015). Comparative modeling of an in situ diffusion experiment in granite at the Grimsel Test Site. *Journal of Contaminant Hydrology*, *179*, 89–101.
- Tachi, Y., Ebina, T., Takeda, C., Saito, T., Takahashi, H., Ohuchi, Y., & Martin, A. (2015). Matrix diffusion and sorption of Cs⁺, Na⁺, I⁻ and HTO in granodiorite: Laboratory-scale results and their extrapolation to the in situ condition. *Journal of Contaminant Hydrology*, *179*, 10–24.
- Tachi, Y., & Yotsuji, K. (2014). Diffusion and sorption of Cs⁺, I⁻ and HTO in compacted sodium montmorillonite as a function of porewater salinity: Integrated sorption and diffusion model. *Geochimica et Cosmochimica Acta*, *132*, 75–93.
- Tachi, Y., Yotsuji, K., Seida, Y., & Yui, M. (2011). Diffusion and sorption of Cs⁺, I⁻ and HTO in samples of the argillaceous Wakkanai formation from the Horonobe URL, Japan: Clay-based modeling approach. *Geochimica et Cosmochimica Acta*, *75*, 6742–6759.
- Toivanen, J. I., Mattila, Hyväluoma, K., Kekäläinen, J., Puurtinen, P. T., & Timonen, J. (2013). Simulation software for flow of fluid with suspended point particles in complex domains: Application to matrix diffusion. In P. Manninen & P. Öster (Eds.), *Applied parallel and scientific computing* (pp. 434–445). Berlin, Germany: Springer.
- Trincherio, P., Molinero, J., Román-Rossa, G., Berglund, S., & Selroos, J.-O. (2015). FASTREACT—An efficient numerical framework for the solution of reactive transport problems. *Applied Geochemistry*, *49*, 159–167.
- Trincherio, P., Painter, S., Ebrahimi, H., Koskinen, L., Molinero, J., & Selroos, J.-O. (2016). Modelling radionuclide transport in fractured media with a dynamic update of K_d values. *Computers & Geosciences*, *86*, 55–63.
- Tsukamoto, M., & Ohe, T. (1993). Effects of biotite distribution on cesium diffusion in granite. *Chemical Geology*, *107*, 29–46.
- Turekian, K. K., & Wedepohl, K. H. (1959). Distribution of the elements in some major units of the Earth's crust. *Geological Society of America Bulletin*, *72*(3), 175–192.
- Videnská, K., Gondolli, J., Stamberg, K., & Havlova, V. (2015). Retention of selenium and caesium on crystalline rock: The effect of redox conditions and mineralogical composition. *Journal of Radioanalytical and Nuclear Chemistry*, *304*, 417–423.
- Vilks, P., Cramer, J., Jensen, M., Miller, N., Miller, H., & Stanchell, F. (2003). In situ diffusion experiment in granite: Phase I. *Journal of Contaminant Hydrology*, *61*(1–4), 191–202.
- Voutilainen, M., Kekäläinen, P., Hautojärvi, A., & Timonen, J. (2010). Validation of matrix diffusion modeling. *Physics and Chemistry of the Earth*, *35*, 259–264.
- Voutilainen, M., Poteri, A., Helariutta, K., Siitari-Kauppi, M., Nilsson, K., Andersson, P., . . . Koskinen, L. (2014). *In-situ experiments for investigating the retention properties of rock matrix in ONKALO, Olkiluoto, Finland*. Paper presented at the WM2014 Conference Proceedings, Phoenix, AZ.
- Voutilainen, M., Sardini, P., Siitari-Kauppi, M., Kekäläinen, P., Aho, V., Mylly, M., & Timonen, J. (2013). Simulated diffusion of tracer in altered tonalite with heterogeneous distribution of porosity. *Transport in Porous Media*, *96*(2), 319–336.
- Voutilainen, M., Siitari-Kauppi, M., Sardini, P., Lindberg, A., & Timonen, J. (2012). Pore-space characterization of an altered tonalite by X-ray computed microtomography and the ¹⁴C-labeled-polymethylmethacrylate method. *Journal of Geophysical Research*, *117*, B01201. <https://doi.org/10.1029/2011JB008622>
- Widestrand, H., Byegård, J., Cvetkovic, V., Tullborg, E.-L., Winberg, A., Andersson, P., & Siitari-Kauppi, M. (2007). Sorbing tracer experiments in a crystalline rock fracture at Äspö (Sweden): 1. experimental setup and microscale characterization of retention properties. *Water Resources Research*, *43*, W10413. <https://doi.org/10.1029/2006WR005277>
- Widestrand, H., Byegård, J., Nilsson, K., Höglund, S., Gustafsson, E., & Kronberg, M. (2010). *Long term sorption diffusion experiment (LTDE-SD): Performance of main in situ experiment and results from water phase measurements* (Tech. Rep. SKB R-10-67). Stockholm, Sweden: Svensk kärnbränslehantering AB.
- Xuan, Y., Zhao, K., & Li, Q. (2010). Investigation on mass diffusion process in porous media based on lattice Boltzmann method. *Heat Mass Transfer*, *46*(10), 1039–1051.
- Zwicky, H.-U., Low, J., & Ekeröth, E. (2011). *Corrosion studies with high burnup light water reactor fuel: Release of nuclides into simulated groundwater during accumulated contact time of up to two years* (Tech. Rep. SKB TR-11-03). Stockholm, Sweden: Svensk kärnbränslehantering AB.